ENGINEERING RESEARCH INSTITUTE
UNIVERSITY OF MICHIGAN

DEPARTMENT OF AERONAUTICAL ENGINEERING

AN AERODYNAMIC METHOD OF MEASURING THE AMBIENT TEMPERATURE OF AIR AT HIGH ALTITUDES

U. S. War Department
Contract No. W-36-039 sc-32307
(Meteorological Branch, Signal Corps)

Department of the Army Project: No. 3-99-07-022
Signal Corps Project: No. 172B

Submitted for the Project By:

Fred L. Bartman
Vi-Cheng Liu
Edward J. Schaefer

UNIVERSITY OF MICHIGAN PROJECT PERSONNEL

Both Part Time and Full Time

Bartman, Fred L., M.S. (EE), Research Engineer
Courtney Howard W., B. S., Research Engineer
Grabowski, Walter, Laboratory Technician
Jones, Leslie M., B. S., Research Engineer
King, Jay B., B.A., Research Assistant
Lally, Frank I., Laboratory Assistant
Leite, Richard J., M.S. (AE), Research Associate
Liu, Vi-Cheng, M.S. (AE), Research Associate
Loh, Leslie, M.S., Chemist
Neill, Howard, M.S., Research Engineer
Nichols, Myron H., PhD, Consultant
Schaefer, Edward J., M.S., Research Engineer
Swets, Maxine, Stenographer-Clerk
Titus, Paul A., Research Technician
Wenk, Norman J., B.S., Research Associate
Wenzel, Elton A., Research Technician
Williams, Ralph O., Research Technician

Errata

1. Page 6, change U to V.

2. Page 7, line 3, change "a non-linear differential equation" to "four non-linear differential equations".

3. Page 11, 4.3c, 4.3d, 4.3e, change "one-tenth" to "one-eighth".

ABSTRACT

The measurement of ambient air temperatures at high altitudes by determination of the shape of the shock cone attached to the nose cone of a rocket that moves at high supersonic speeds is described. Data from the trial of the method on V-2 Number 56 are analyzed on the basis of first order conical shock wave theory. On V-2 Number 56 Pirani gauge signals were obtained up to 230,000 feet indicating that the method may be applicable up to this altitude. Temperatures calculated for altitudes up to 183,000 feet agree fairly well with what was previously known about temperatures at high altitudes.

The experimental errors are shown to be negligibly small. The possible existence of large systematic errors and plans for investigating them are discussed.

The use of this method for measurement of winds at high altitudes is discussed.

TABLE OF CONTENTS

TABLE OF CONTENTS (Continued)

ILLUSTRATIONS

ILLUSTRATIONS (Continued)

TABLES

NOTATION

V Air speed which is equal to the missile velocity relative to the atmospheric air.

a Speed of sound.

M Free stream Mach number.

ℓ Mean free path of the fluid (air).

L Characteristic length of the body.

δ_1 Thickness of the boundary layer.

μ Viscosity coefficient.

ρ Fluid (air) density.

Re Reynolds number which is equal to $\frac{VL\rho}{\mu}$

$\bar{c}$ Average molecular speed which, for air, is equal to $\sqrt{\frac{8}{\pi\gamma}}\, a$ (Ref. 10).

γ Ratio of specific heat at constant pressure to the specific heat at constant volume, for air $\gamma = 1.405$.

θ_s Semi-apex angle of nose cone.

θ_w Shock wave angle of the non-yaw cone at corresponding free stream Mach number.

ϵ Angle of yaw of nose cone (ϵ is equal to the angle between axis of nose cone and the free stream velocity vector of the air.

$\delta = \alpha\epsilon$ Where δ is the angle of yaw of the shock cone. (δ is equal to the angle between the axis of the shock cone and the free stream velocity vector of the air.

r, θ, ϕ Polar Coordinates in Figure 2.

$\phi = \epsilon - \delta$ angle of yaw between shock cone and missile axis.

β_0, β_2 Constants used in equation 4, see (R14).

NOTATION (Continued)

$\Delta\theta_W$	Change in semi-apex angle of shock cone in yawed case (second order theory).
θ_W'	Semi-apex angle of shock cone in yawed case (second order theory).
x,y,z	Rectangular cartesian coordinates in system which is fixed in the nose cone of the rocket.
ξ	An azimuth angle in Fig. 34.
M_o	Gram molecular weight of a gas.
P_{θ_W}	Propable error in θ_W.
P_x, ... etc.	Probable error in x.
α_i	Equal to $\sqrt{x_i^2+y_i^2+z_i^2}$
T	Temperature degrees Kelvin
$T_{0.1}$	Time required to complete one-tenth of an exponential change.
A,B,C	Vectors in Fig. 37.
W	Wind velocity vector in Fig. 37.
η	An azimuth angle in Fig. 37.

AN AERODYNAMIC METHOD OF MEASURING THE AMBIENT TEMPERATURE OF AIR AT HIGH ALTITUDES

1. INTRODUCTION

It is the purpose of this experiment to measure the ambient kinetic temperature of air at high altitudes by an aerodynamic method. This consists of measuring the angle of the shock wave (the "weak" shock or the "first" solution of the conical flow equations) attached to the nose cone of a missile that moves at high supersonic speeds. The shock wave is located by signals obtained from Pirani gauge probes which are moved up and down through the shock wave. The method depends only upon the determination of the time of the signal and not upon the amplitude of the signal. The missile velocity relative to earth is obtained by optical tracking or Doppler (R1)[1]. The missile velocity relative to the air can be obtained if the wind velocity is known.

From the aerodynamics of an ideal fluid, it is known that the angle of a shock wave attached to a slightly yawing semi-infinite cone is a unique function of the free stream Mach number of the air flow around the cone (R2). Mach number is defined as the ratio of the air speed to the speed of sound. The latter is known to be a unique function of air temperature. Since the air speed is equal to the missile velocity relative to air, one can determine the ambient air temperature in terms of the corresponding shock wave angle.

2. HISTORY OF THE EXPERIMENT

The measurement of upper atmosphere ambient temperatures by determination of the geometry of the shock wave off the tip of a rocket was suggested at an early meeting of the V-2 Panel. The probe method for measuring a shock wave from a conical tip, described above, has been flown on three V-2 rockets, Numbers 33, 50, and 56. An optical method, photographing the shock wave from a wedge-shaped rocket tip by means of a shadowgraph system, was tried on V-2 rocket Number 42.

V-2 Number 33 was launched on September 2, 1948. Although the missile reached a high altitude, the telemetering unit failed 18 seconds after take-off and was completely inoperative thereafter except for a two-second interval at fifty seconds. No data were obtained from this flight (R3).

---

[1] See References, Section 11.

V-2 number 50 was launched on April 11, 1949. The Pirani gauges, which are the sensitive elements in the tips of probes, failed shortly after the experiment started, and therefore only a small amount of data was obtained (R4).

Improved gauges were flown on V-2 number 56 on November 18, 1949. Excellent data were obtained from all four Pirani gauges in the altitude range between 85,000 and 130,000 feet. One of the gauges or its circuit failed at this point. Data were obtained from the other three gauges up to 145,000 feet, when a second gauge or circuit failure occurred. Signals were obtained from the remaining two gauges up to 230,000 feet, demonstrating the feasibility of the experiment up to this altitude (R5). The premature failure of the two gauges or their circuits was possibly due to the misfire of a sound grenade from the SCEL temperature experiment which was also flown on this missile.

The shadowgraph optical method used on V-2 number 42 (December 9, 1948) did not give any results because of a switch or power failure. Subsequent tests of shadowgraph and schlieren methods in the low pressure supersonic wind tunnel at the NACA laboratories at Langley Field, Va. were made in April, 1949. The tests indicated that shock wave photographs might be obtained up to 130,000 feet with a shadowgraph system and up to 170,000 feet with a schlieren unit, with an accuracy of about $\pm$ 3°C up to 98,000 feet. (R6). Inasmuch as the probe experiment showed promise of obtaining shock wave data at much higher altitudes, the optical methods were shelved at this time.

3. STONE'S THEORY OF SUPERSONIC FLOW AROUND YAWING CONES AND ITS LIMITATIONS IN APPLICATION

When a missile is moving in air at a high supersonic speed, a shock wave attached to its nose cone is formed. With several plausible assumptions, Stone's theory of supersonic flow around yawing cones gives the relation between shock wave angle and the corresponding free stream Mach number.

3.1 Discussion of the Assumptions

The assumptions that have to be made in order that Stone's theory can be applied are as follows:

3.11 Air is a Continuous Medium

From the kinetic point of view, the realms of the mechanics of flow can be divided into three regions: (a) continuum flow, (b) slip flow, (c) free molecular flow. These flow regions can be characterized as follows: In continuum flow, the mean free path ℓ of the fluid is negligibly small compared to the size of the body L. In free molecular flow ℓ is large compared to L so that the effect due to intermolecular collisions can be ignored. The slip flow region can be considered as the transition region between continuum flow and

free molecular flow. In this region ℓ is small but not negligible compared to L hence the intermolecular collisions and the collision between the molecules and the body are of equal importance.

Different dimensionless parameters have been suggested as criteria in defining the regions of flow. $\frac{\ell}{\delta_1}$ was used by Tsien (R7) (δ_1 corresponds to δ in R7); $\frac{Re}{M^2}$ by Roberts (R8). It is evident that both are inadequate as far as defining the free molecular flow is concerned because neither the boundary layer nor the definition of Reynolds number exists in the free molecular flow region.

The original parameter, $\frac{\ell}{c}/\frac{L}{V}$, from which Roberts' criterion is derived, can also be reduced to the form $\sqrt{\frac{\pi\gamma}{8}}\frac{\ell}{L}M$ (R15). If

$$0.01 < \frac{\ell}{L} M < 100 \qquad (1)$$

is considered as the proper range for the slip flow region, the boundary of flow regions can be shown as in Figure 1. It is seen that the atmospheric air below 240 thousand feet altitude can be considered as a continuous medium when the Mach number of flow is less than 4. Note that for figure 1, L is assumed to be 1.25 feet. ℓ is taken from Grimminger's tables (R9).

3 .12 Air is Non-viscous

The viscosity influence on the flow is in the form of viscous stress which can be expressed, in the continuous medium, as the product of the viscosity coefficient and the velocity gradient. The magnitude of the viscous force is negligibly small compared to the inertia force acting on the same element of fluid, if an unusually high velocity gradient does not exist. In other words, air can be considered as non-viscous except in the "high velocity gradient" region.

The existence of high velocity gradient in the immediate neighborhood of the body is the cause of "boundary layer flow" in which the order of magnitude of the viscous effect and that of the inertia effect are approximately the same. It has been shown in boundary layer theory that the thickness of the boundary layer δ_1 can be expressed by the relation (R23)

$$\frac{\delta_1}{L} \sim \frac{1}{\sqrt{Re}} \qquad (2)$$

With ordinary density, δ_1/L is in the order of magnitude of 10^{-3}. Hence the assumption of zero boundary layer thickness is justifiable. In other words, air of ordinary density can be considered as non-viscous.

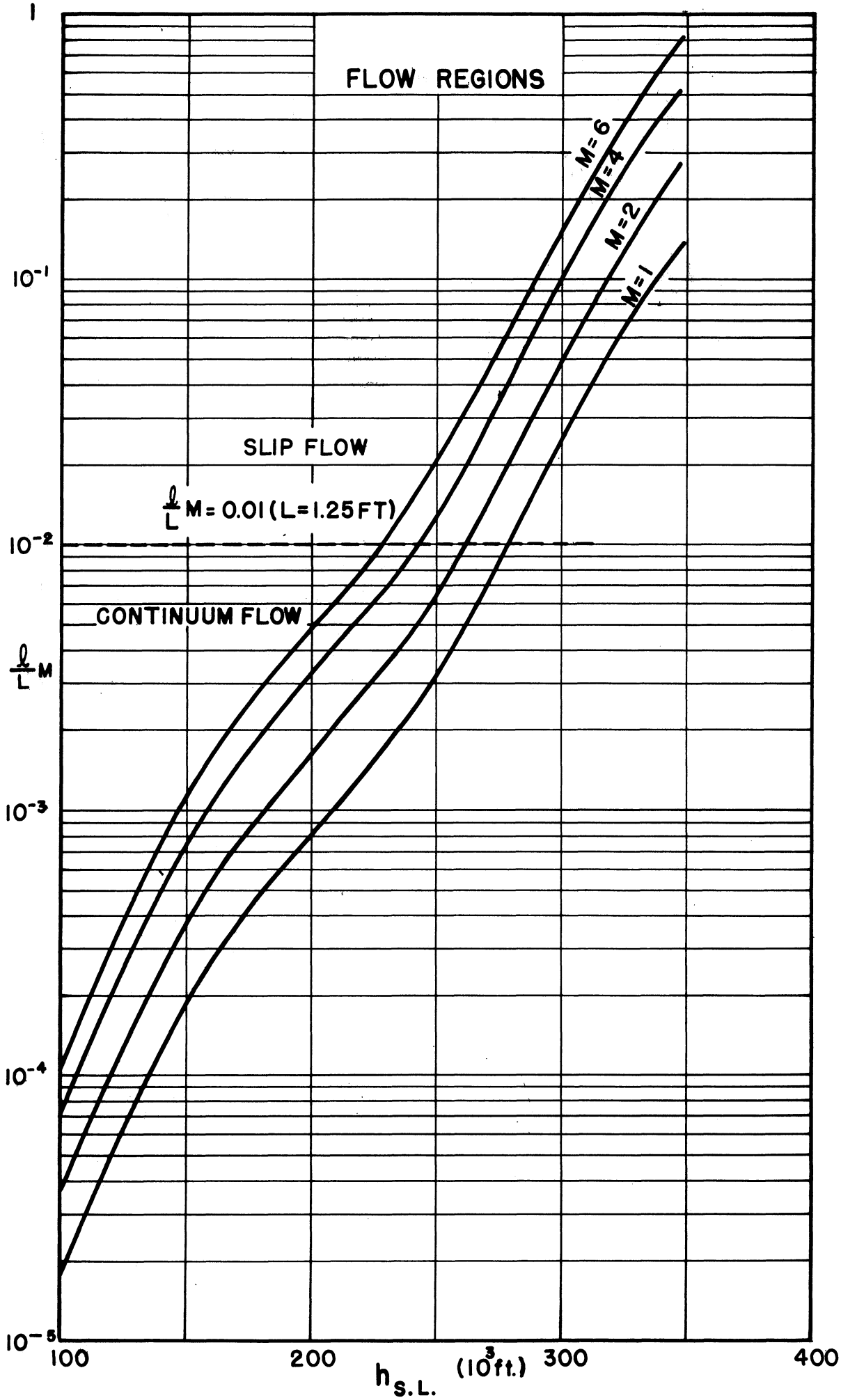

Fig. 1

Flow Regions

It is expected, however, that when the air density decreases to a very low value at high altitudes, the assumption of zero boundary layer thickness will no longer be valid. The range of validity of this assumption will be investigated by the low density wind tunnel test. (See Section 9.2).

3.13 The Ratio of Specific Heats, γ, is Constant and Equal to 1.405.

The ratio of specific heat at constant pressure to that at constant volume for sea level air is 1.405. It has been found through the sampling experiment (R10) that atmospheric air composition remains the same as that of sea level air up to 60 kilometers altitude. It is assumed that dissociation of oxygen and nitrogen is negligible below 80 kilometers (R9).

3.14 The Missile Flies at High Supersonic Speeds.

The missile speeds must be high enough so that the flow is locally supersonic in the region between the conical shock wave off the nose and the expansion wave off the truncated shoulder. For a cone of 20° semi-apex angle, the free stream Mach number should be greater than 1.35. Under this condition and assumption 3.12, the conical flow field around the nose cone will be the same as if the cone were semi-infinite. It is for the semi-infinite cone that Taylor-Maccoll theory, on which Stone's theory is based, is developed.

3.15 Heat Transfer Between the Air Stream and the Body is Negligible.

As mentioned in 3.12, there is a boundary layer region in the immediate neighborhood of the missile in which a high velocity gradient exists. Boundary layer theory shows that a high temperature gradient exists in this region as a consequence of the high velocity gradient. According to the boundary layer theory, the temperature gradient drops to zero at the outer edge of the boundary layer; i.e., at the junction between the "ideal fluid" region and the boundary layer flow region. In other words the boundary layer has an insulated surface at its outer edge. Therefore the heat transfer between the missile and the air due to conduction and convection has no effect on the flow in the "ideal fluid" region to which the conical flow theory applies.

Another source of heat transfer between the missile and the air is radiation. It is estimated that the maximum skin temperature of the nose cone during flight is in the order of 300°F (R11). In absolute temperature units, the maximum skin temperature is less than twice the average air temperature in the "ideal fluid" region. Considering that the air particles flow by the nose cone in less than two thousandths of a second, it is assumed that the effect on the air flow due to radiation from the missile is negligible.

3.2 Brief Description of Conical Flow Theory.

Consider the conical flow around a yawing cone (See Fig. 2) in a rectangular system of coordinates (1, 2, 3) where r, θ, ϕ denote the usual spherical polar coordinates.

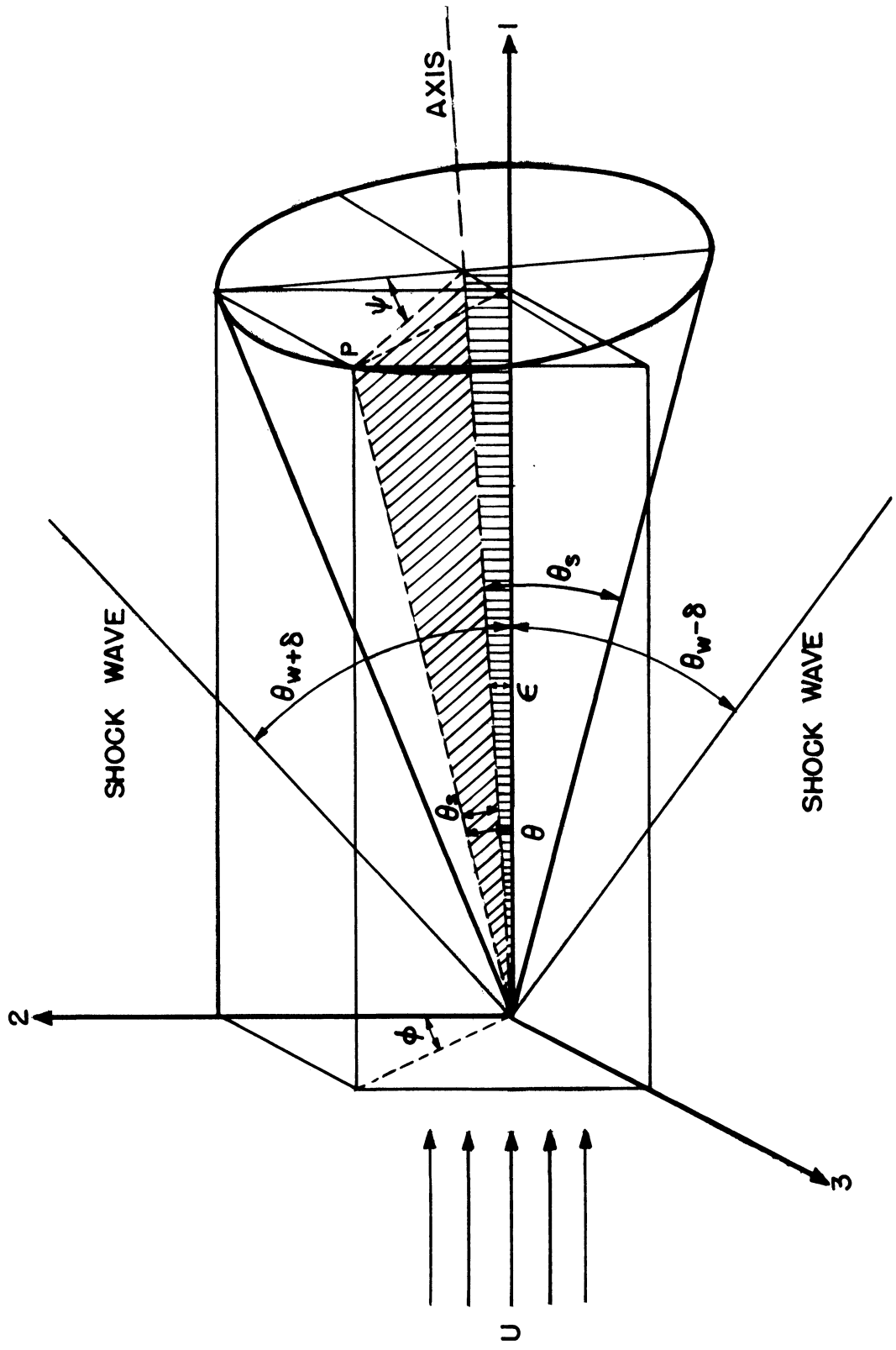

Fig. 2
Yawed Cone In Supersonic Flow

The equations of motion and the continuity equation with the particular boundary conditions of the yawed cone constitute a two-point boundary value problem with a non-linear differential equation. The exact solution of this problem has not yet been developed. The approximate solution has been given by Stone who considers the effects of yaw on the quantities characteristic of the conical flow as perturbations of the corresponding quantities of the non-yaw case. If third and higher order effects of yaw are ignored, the equation of the nose cone and shock wave cone can be reduced to (R14):

$$\theta_s' = \theta_s + \epsilon \cos\phi - \frac{1}{2}\epsilon^2 \cot\theta_s \cdot \sin^2\phi \tag{3}$$

and

$$\theta_w' = \theta_w + \epsilon\alpha \cos\phi + \epsilon^2(\beta_0 + \beta_2 \cos 2\phi) \tag{4}$$

respectively. $\theta_w, \alpha = \frac{\delta}{\epsilon}, \beta_0, \beta_2$ are shown as functions of the free stream Mach number in Fig. 3 and Fig. 4 (R12, R13, R14).

It can be seen from equation 4 that if the angle of yaw is so small that the second order effect of yaw is negligible compared to the first order effect, the shock wave attached to a yawing cone in supersonic flight continues to be a circular cone, of the same apex angle as in the non-yaw case, but with a yaw of its own given by:

$$\delta = \alpha\epsilon \tag{5}$$

The plane of yaw of the shock wave will be the same as the plane of yaw of the cone.

However, with yaw so large that the second order effect must be considered, the shock wave cone ceases to be a circular cone. Its normal cross-section becomes actually a curve of the sixth degree, simulating closely an ellipse of small eccentricity. The magnitude of the second order effect can be obtained from equation (4) above. The semi apex angle of the shock cone in the second order case is given by

$$\theta_w' = \frac{\theta_w'(\phi) + \theta_w'(\phi + \pi)}{2} \tag{6}$$

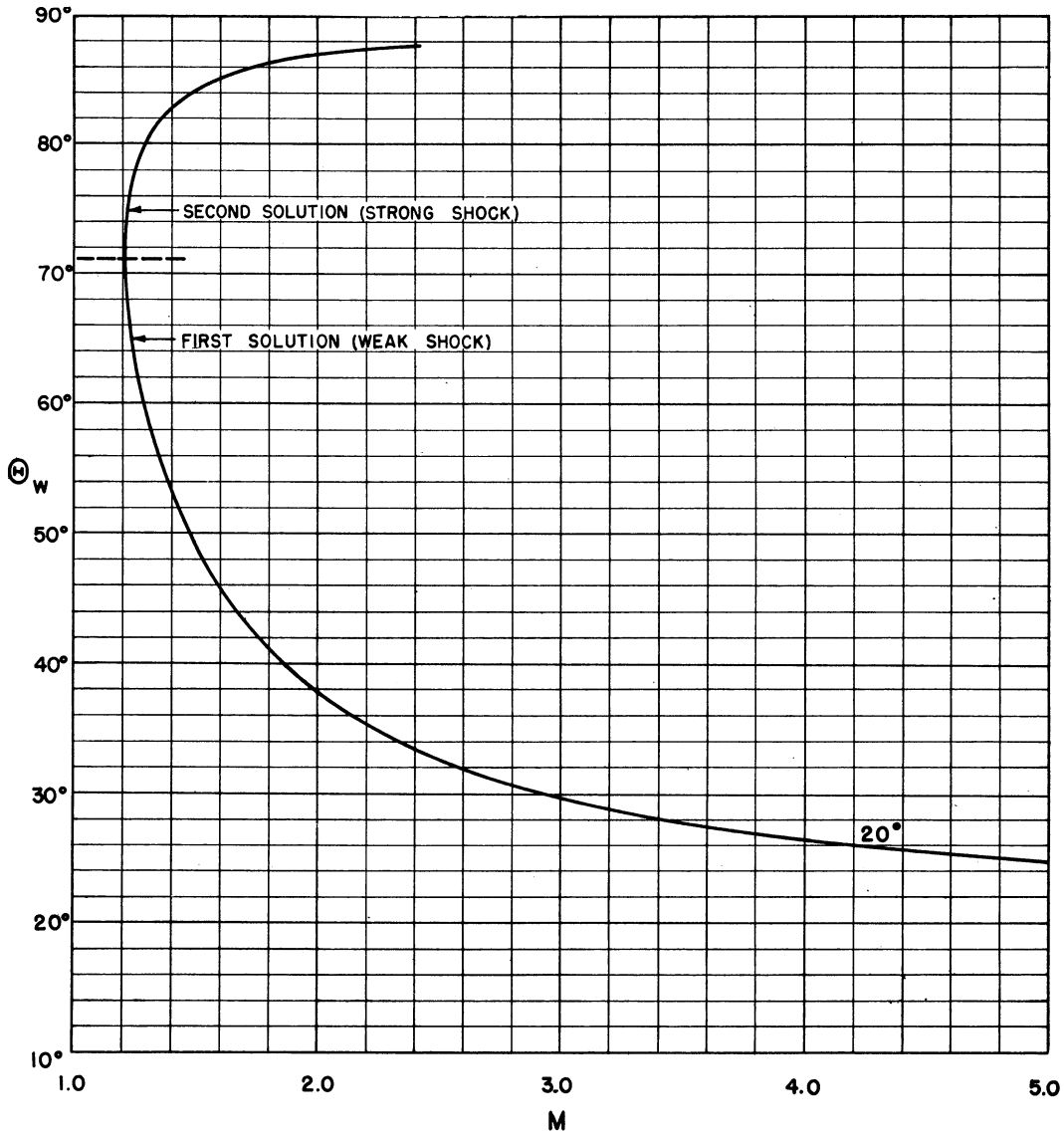

FIGURE 3 WAVE ANGLE FOR A CONICAL SHOCK ATTACHED TO A NOSE CONE OF 20 DEGREE SEMI-INCLUDED ANGLE.

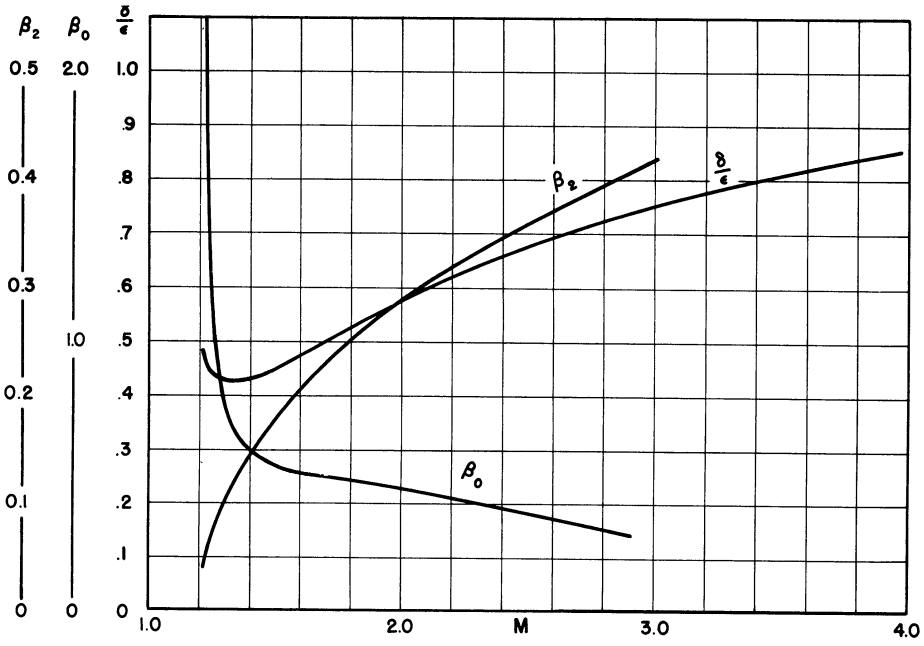

FIGURE 4 δ/ϵ, β_0, β_2 Curves

From (4) above we see that this is equal to

$$\theta_w' = \theta_w + \epsilon^2(\beta_0 + \beta_2 \cdot \cos 2\phi) \tag{6a}$$

The amount by which this varies from the first order case is:

$$\Delta\theta_w = \theta_w' - \theta_w = \epsilon^2(\beta_0 + \beta_2 \cdot \cos 2\phi) \tag{7}$$

This quantity is a maximum for $\phi = 0$, and a minimum for $\phi = \frac{\pi}{2}$. The maximum and minimum values of $\Delta\theta_w$ are respectively:

$$\Delta\theta_{w_{max}} = \epsilon^2(\beta_0 + \beta_2)$$

$$\Delta\theta_{w_{min}} = \epsilon^2(\beta_0 - \beta_2) \tag{8}$$

Table 1 gives the values of these quantities for angles of yaw up to 10 degrees, for a cone of 20° semi apex angle, with free stream Mach number equal to 2.839.

β_0 and β_2 were obtained from (R14). The curves of β_0 and β_2 against Mach number for a 20° semi apex angle cone (Fig. 4) show that they vary slowly for Mach numbers between 2 and 4 so that the values of $\Delta\theta_w$ given in table 1 are approximately correct for Mach 4.

TABLE 1

SECOND ORDER CORRECTIONS TO θ_W

$\theta_s = 20^\circ$
$M = 2.839$
$\beta_o = 0.29$
$\beta_2 = 0.40$
$\theta_W = 30.44^\circ$

$\Delta\theta_{Wmax} = \epsilon^2(\beta_o + \beta_2) = 0.69\epsilon^2$

$\Delta\theta_{Wmin} = \epsilon^2(\beta_o - \beta_2) = -0.11\epsilon^2$

ϵ Deg.	ϵ Radians	ϵ^2	$\Delta\theta_{Wmax}$ Radians	$\Delta\theta_{Wmax}$ Degrees	$\Delta\theta_{Wmin}$ Radians	$\Delta\theta_{Wmin}$ Degrees
0	0	0	0	0	0	0
1	.01745	.0003045	.00021	.012	-.0000335	-.00192
2	.03491	.00122	.00084	.048	-.000134	-.00768
3	.05236	.00274	.00189	.108	-.000301	-.0172
4	.06981	.00487	.00336	.193	-.000536	-.0307
5	.08727	.00762	.00526	.301	-.000838	-.048
7.5	.13091	.01714	.01183	.678	-.00189	-.108
10	.17453	.03046	.02102	1.204	-.00335	-.192

4 . MODEL TEST OF THE PROBE METHOD

4.1 Statement of the Problem

Although optical methods have been commonly used in detecting shock waves, their value on a rocket is small because of the technical difficulties involved and because of their low sensitivity at high altitudes. In view of these shortcomings it was decided to use probes containing a pressure sensitive element. Because of their sensitivity Pirani gauges seemed to be suitable for detecting shock waves in a low density flow field. A check on the suitability of the method was desirable.

4.2 Purpose of the Test

To examine the suitability of Pirani gauge pressure probes for detecting shock waves in the following ways:

a) Take Schlieren photographs to see if the shock wave to be detected is distorted by the probe.
b) Record signals from the Pirani gauges on a Brush recorder and correlate with the above photographs to see how well they define the shock wave position.

4.3 Apparatus

a) University of Michigan supersonic wind tunnel.
b) A Schlieren system and a Fastax camera.
c) One-eighth scale model of a V-2 nose cone with a reciprocating probe and facilities for a one-tenth scale probe or a full size probe.
d) One-tenth scale impact probe.
e) One-tenth scale static probe.
f) Full size impact probe and one channel of associated electronic apparatus similar to that installed on V-2 No. 33.
g) Two channel Brush recorder; one channel for recording pressure signals from Pirani probe, the other for recording the 60 cycles A.C. voltage used to flash a neon bulb in the camera for correlation between the pressure record and the photographs.

4.4 Test Conditions

The experiment consisted of three series of tests, one for each probe model. In each series, three different angles of attack: 0°, $+ 12^{\circ}$, $- 12^{\circ}$, were used. The test Mach number was 1.93; the test section pressure was about 100 mm. Hg. Schlieren photos were taken at 700 frames per second.

4.5 Results and Conclusions

Correlation between the pressure record and photographs indicated that a signal was given by the Pirani gauge when the point on the gauge inlet orifice closest to the shock wave actually came in contact with the wave. Therefore when the probe was moving forward the signal was received when the point on the Pirani gauge opening most distant from the axis of the cone came in contact with the shock wave from the cone and on the return excursion when the point closest to the cone axis came in contact with the shock wave. Figures 5, 6, 7 show portions of the Brush records. It should be noted that the above conclusion is subject to the possible error due to the distortion of the shock wave by the presence of the probe in the flow field. This error could change in both sign and magnitude when the direction of probe motion is reversed. However, it was found that the shock wave angle, with the probe at its signal-issuing position, checked with the theoretical results (with no probe present) within the experimental accuracy which was in the order of $\pm 0.5^{\circ}$. Hence any possible error in the shock wave angle due to distortion of the shock wave with this method should be less than $\pm 0.5^{\circ}$.

Figures 8 to 16 show the Schlieren photos for different probes at different angles of attack.

The static probe appeared to give smaller distortion to the shock wave. However, the pressure signals obtained from a static probe (R4) are not as sharp as those from an impact probe. This is because the shock wave, hence the pressure discontinuity, can occur only when the local velocity is supersonic. Due to the existence of boundary layer in which velocity builds up from zero at the wall to main stream value at the outer edge of the boundary layer, there is no pressure discontinuity in a thin layer of flow in the immediate neighborhood of the static probe.

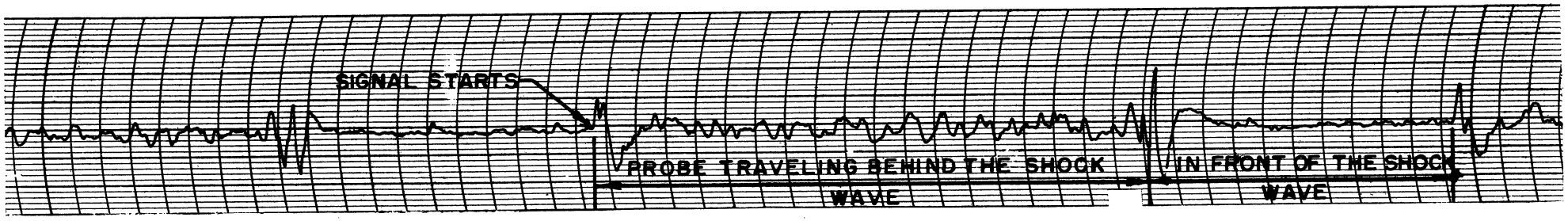

FIGURE 5. BRUSH RECORD, + 12° YAW

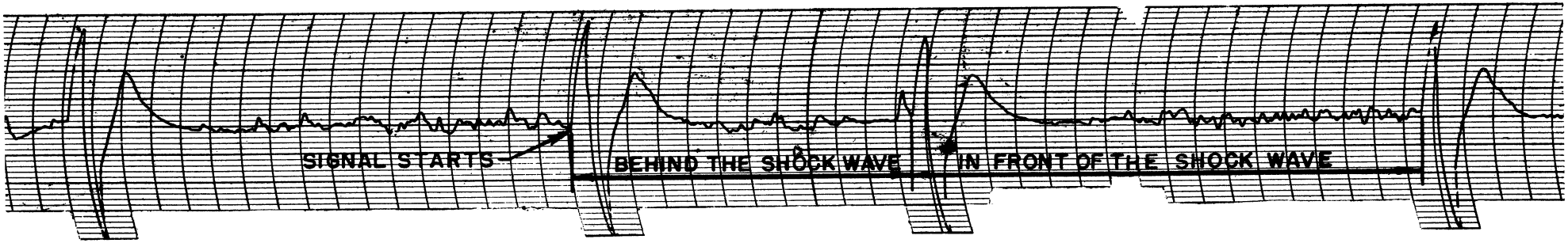

FIGURE 6. BRUSH RECORD, − 12° YAW

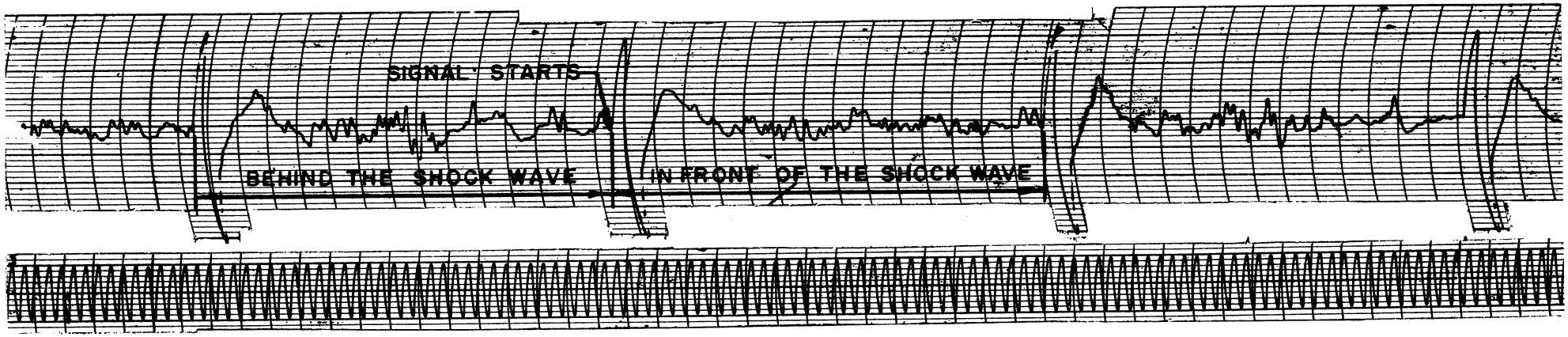

FIGURE 7. BRUSH RECORD, 0° YAW AND 60 CYCLE TIMING WAVE.

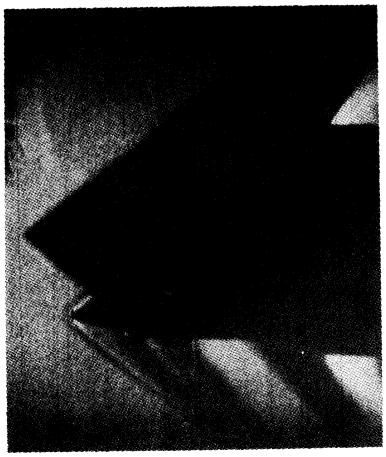

FIG. 8
PIRANI PROBE, 0°

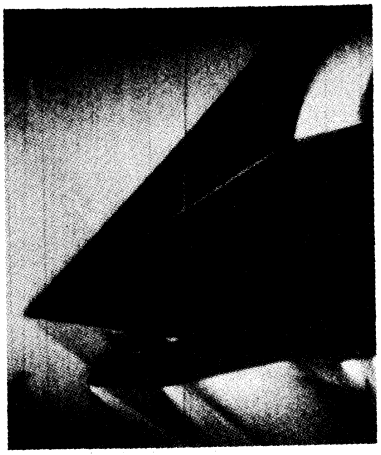

FIG. 9
PIRANI PROBE, +12°

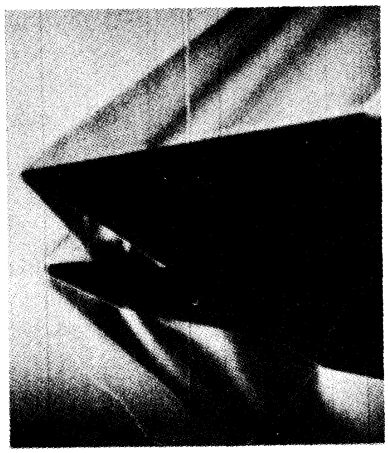

FIG. 10
PIRANI PROBE, -12°

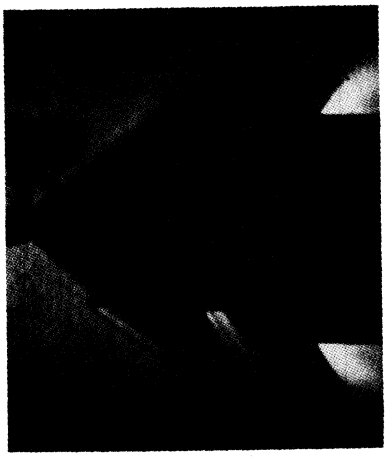

FIG. 11
SCALE IMPACT PROBE, 0°

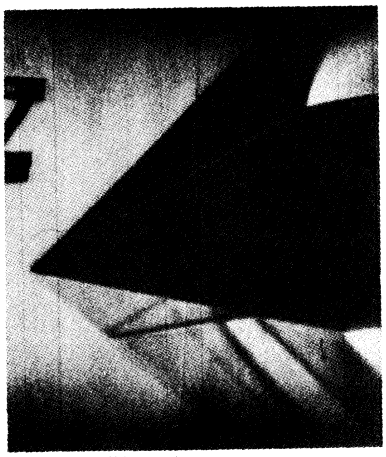

FIG. 12
SCALE IMPACT PROBE, +12°

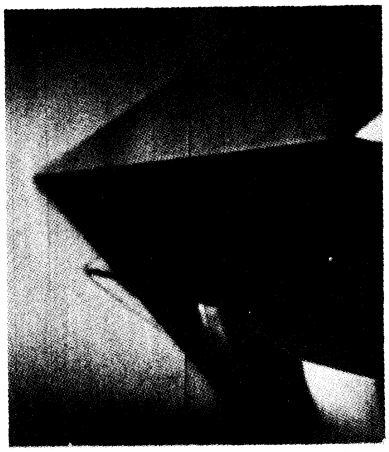

FIG. 13
SCALE IMPACT PROBE, -12°

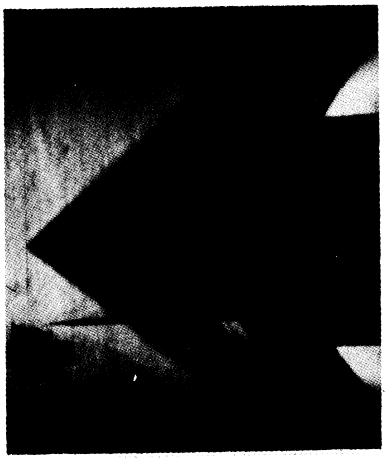

FIG. 14
SCALE STATIC PROBE, 0°

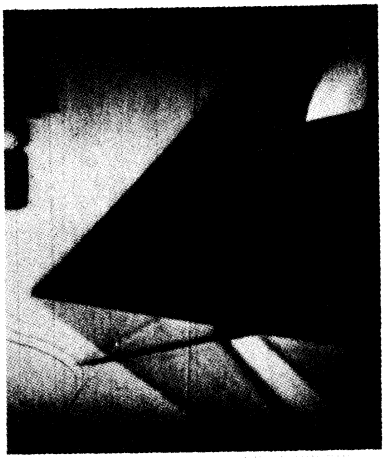

FIG. 15
SCALE STATIC PROBE, +12°

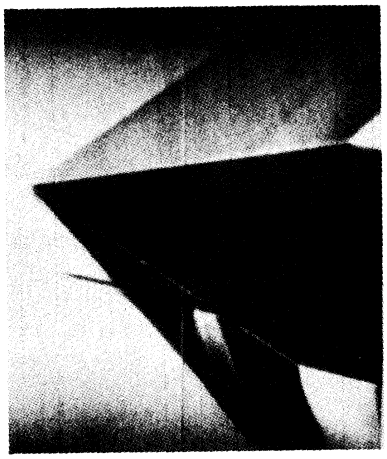

FIG. 16
SCALE STATIC PROBE, -12°

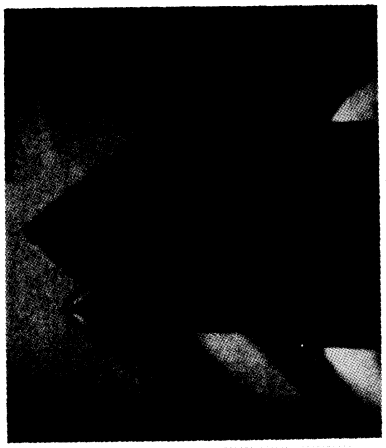

FIG. 8
PIRANI PROBE, 0°

FIG. 9
PIRANI PROBE, +12°

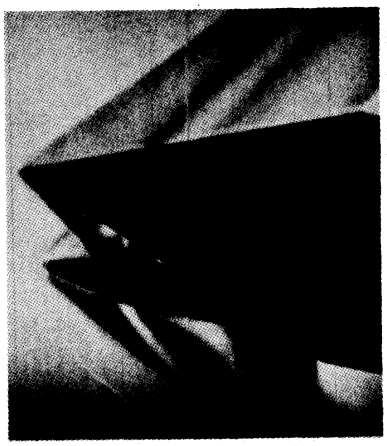

FIG. 10
PIRANI PROBE, -12°

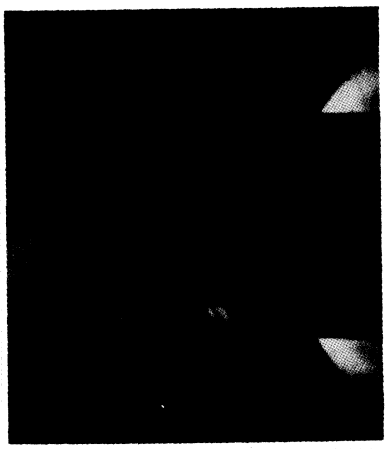

FIG. 11
SCALE IMPACT PROBE, 0°

FIG. 12
SCALE IMPACT PROBE, +12°

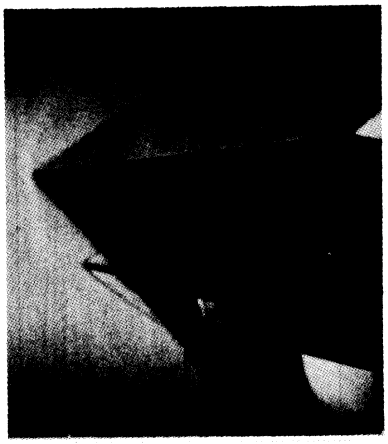

FIG. 13
SCALE IMPACT PROBE, -12°

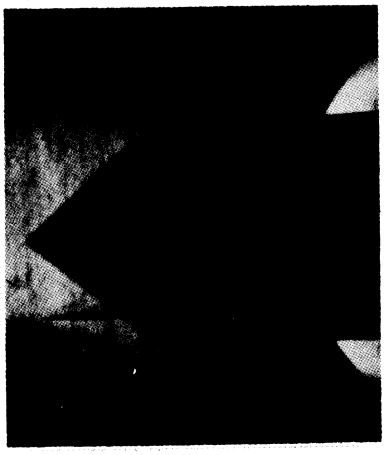

FIG. 14
SCALE STATIC PROBE, 0°

FIG. 15
SCALE STATIC PROBE, +12°

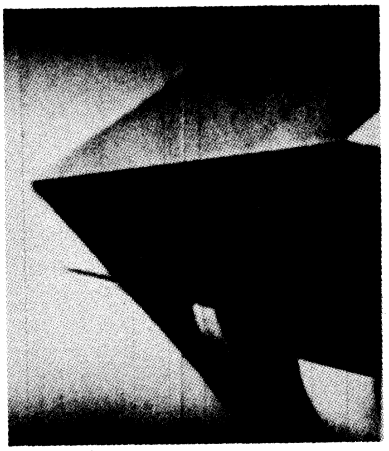

FIG. 16
SCALE STATIC PROBE, -12°

5. APPARATUS USED ON V-2 NUMBER 56

5.1 Mechanical

The apparatus used on V-2 Number 56 is shown in Fig. 17. The nose of the missile was an accurately machined right circular cone having a 40 degree included angle. It was 33 inches long. The four probes, placed symmetrically at 90 degree intervals around the cone, protruded from the cone surface at points 8 inches from the cone axis and 21.5 inches from the tip of the cone. They moved up and down in unison through a distance of 8 inches in a line parallel to the cone axis. The region of travel 9.6 to 17.2 inches from the tip of the cone was calibrated; making possible the measurement of shock cones having 25 to 40 degree semi-apex angles.

In order to avoid possible damage to the probes by excessive heating or turbulance they remained recessed below the bushings which covered the probe openings until 57.6 seconds after take-off (altitude 85,000 feet). At this time the probes started oscillating with a period of 3 seconds. After the second cycle the period decreased and varied between 2.69 and 2.84 seconds for the rest of time during which shock wave signals were obtained. The speed of the motion (during each half cycle) was essentially uniform for the calibrated portion of the probe travel. The acceleration necessary to reverse the direction of probe travel was confined to the uncalibrated end portions of the motion.

The speed of the rocket varied between 3600 and 4380 feet per second for the period of time during which shock wave data were obtained. Thus the shock angle was measured twice in each 10,000 to 12,000 feet of rocket travel.

The nose cone was oriented on the rocket so that the probes were in line with the rocket fins; that is, probe 1 was in line with fin 1 (pointing north when the rocket was fired); probe 2, with fin 2 (west); probe 3, with fin 3 (south); and probe 4, with fin 4 (east).

5.2 Pirani Gauges

Two slightly different kinds of Pirani gauges were used in the probes on V-2 Number 56. Figures 18 and 19 show the probe construction. The sensitive element in each probe was a very fine platinum wire (Pirani gauge). Two of the gauges were of 0.0001 inch diameter wire, .375 inches long; and two were of 0.0002 inch diameter wire, .75 inches long. The tip of each probe had a circular opening .094 inches in diameter.

The pressure of the air inside of the probe cavity, i.e., of the air surrounding the Pirani wire, is essentially Pitot tube pressure during flight. (The term "Pitot tube pressure" is used for the stagnation pressure behind the normal shock which exists in front of the probe tip). Stone's theory shows that the Pitot tube pressure is smaller in front of the shock wave than it is behind the shock wave. When the tip of the probe passes through the region in which the Pitot tube pressure change takes place, the change of pressure inside of the probe cavity is accompanied by a change in resistance of the Pirani wire.

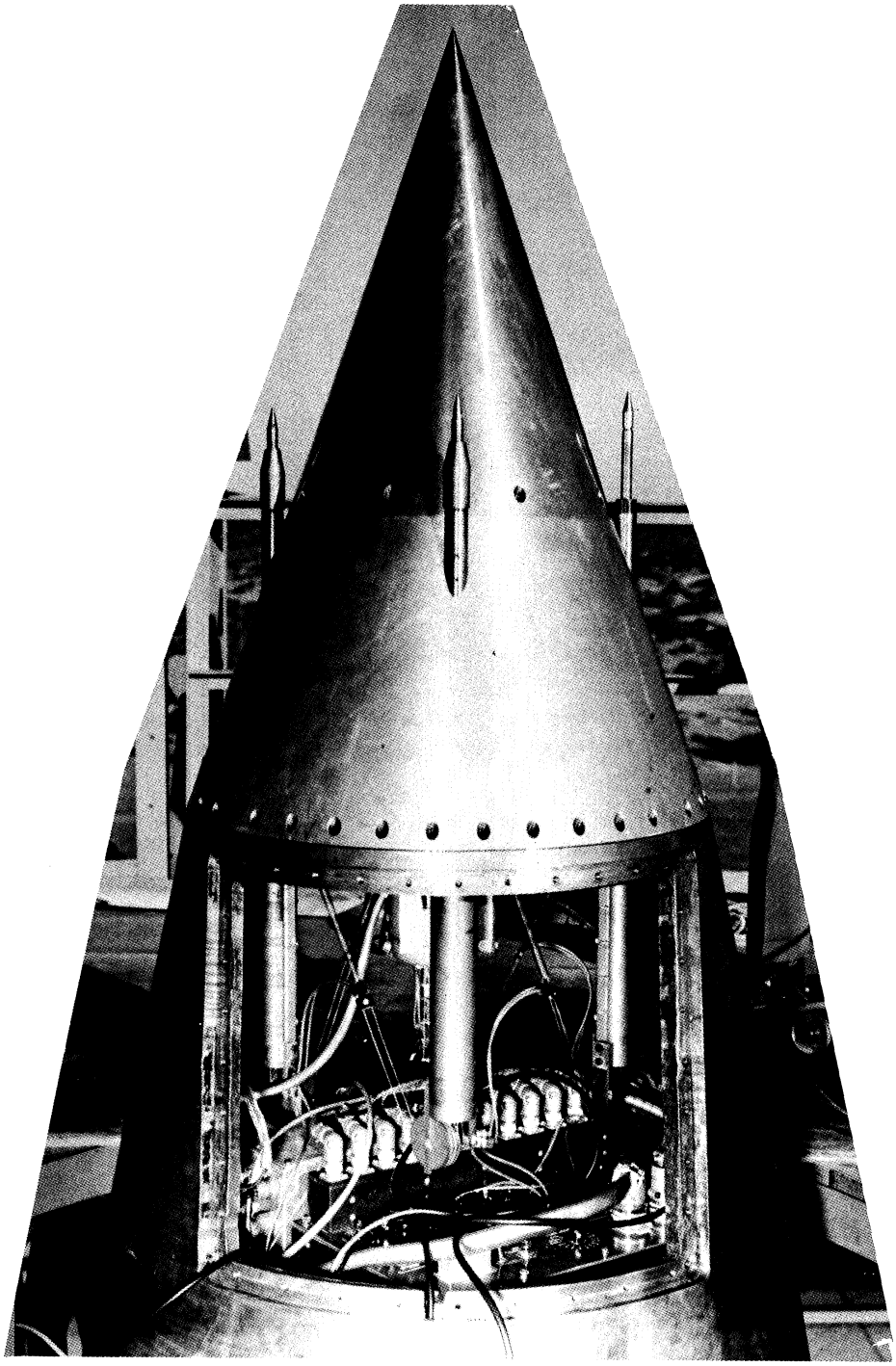

Fig. 17

Apparatus Used on V-2 Number 56

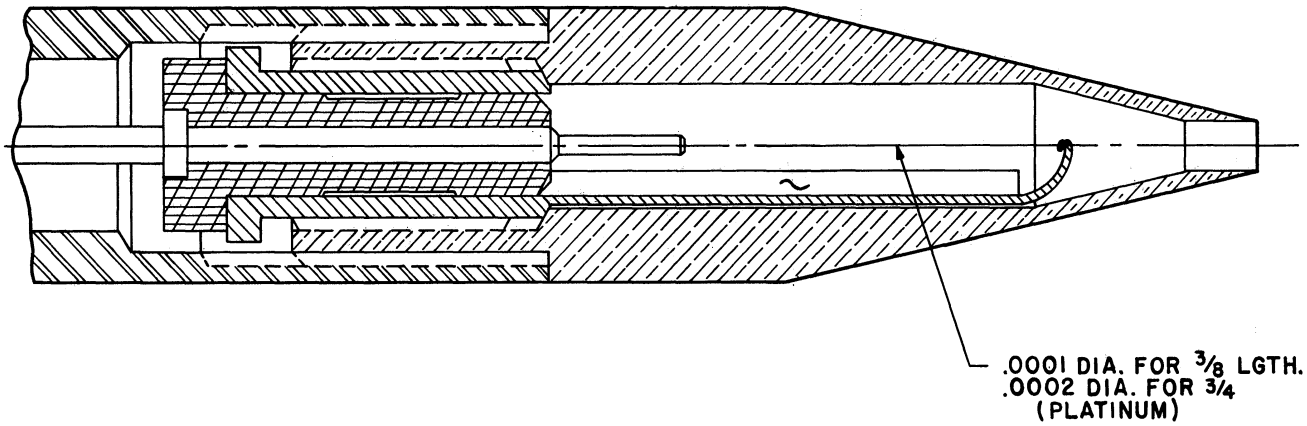

FIG. 18

PIRANI GAUGES USED
ON V-2 NUMBER 56

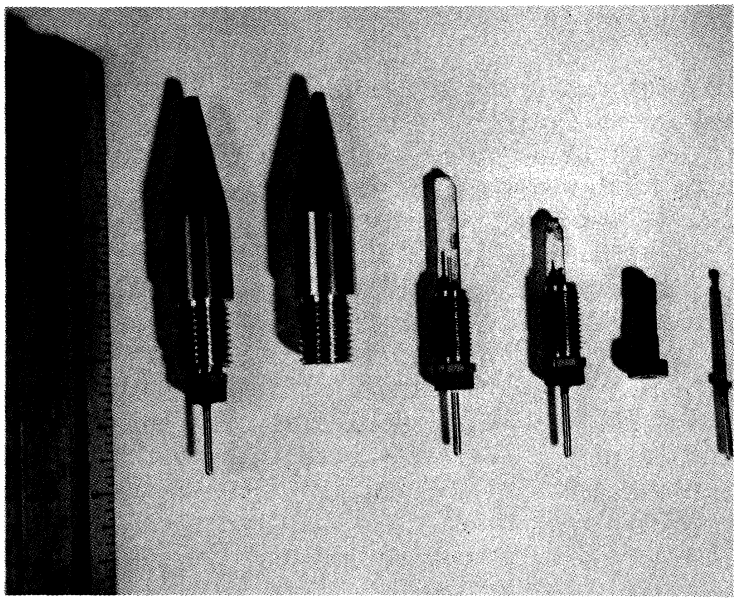

Fig. 19

Photo of Pirani Gauges Used on V-2 Number 56

Each wire was operated in series with a battery and resistance as shown in Fig. 20. Thus the change in resistance of the Pirani wire caused a change in the voltage across the Pirani wire. This electrical signal was amplified and applied to the recording systems.

The static characteristic curves of the Piranis are shown in Fig. 21. The data were obtained in the following way. The Pirani was mounted in a cavity similar to that used on V-2 number 56. The cavity was connected to a vacuum system and the Pirani was connected into the circuit of Fig. 20. The pressure of the air surrounding the Pirani was decreased in steps. Under equilibrium conditions at each step, the pressure was measured with a Mc Leod gauge while the Pirani voltage was determined with a Leeds and Northrup type K-2 potentiometer. From the curves it can be seen that the greatest sensitivity was obtained in the range of pressures between 0.5 and 100 mm. of Hg.

The Pitot tube pressures theoretically encountered on a typical flight and the corresponding expected Pirani signals are shown in Table 2. These calculations were made for a flight with 120 km. (394,000 feet) peak altitude. The peak altitude on V-2 number 56 was 405,700 feet.

The time constant (defined as the time required to complete 63% of the voltage change caused by a rapid change in air pressure) of a Pirani gauge of the type described above is determined by two factors; the time required for the pressure change at the tip of the probe to propagate into the cavity, and the time required by the hot wire to change its resistance after the air pressure inside of the cavity has changed.

The time constants of gauges similar to those used on V-2 number 56 were investigated experimentally in two ways. In the first method a solenoid operated bellows was used to produce a pressure change at the opening of the probe. The resulting change of voltage across the Pirani was recorded with a Hathaway oscillograph through a cathode follower circuit. (See Fig. 22). Because the mechanical system itself required 17 to 33 milliseconds to operate, the time constants determined with this method are higher than the true values. A lower limit for the gauge time constant was arrived at with a second method. This consisted of applying a square wave of voltage to the Pirani wire and observing the change in Pirani current on a cathode ray oscilloscope. The time constants determined with this method are smaller than the true values because that portion of the time constant due to propagation of the pressure change into the cavity has been neglected.

The average values of these measurements are plotted in Fig. 23. The measurements were made for Pirani gauges 0.5 inch in length. The investigation also showed that for a given diameter of wire increasing the length decreased the time constant, whereas decreasing the length increased the time constant. The 0.0002" diameter wires which were used on V-2 number 56 were .75 inches long.

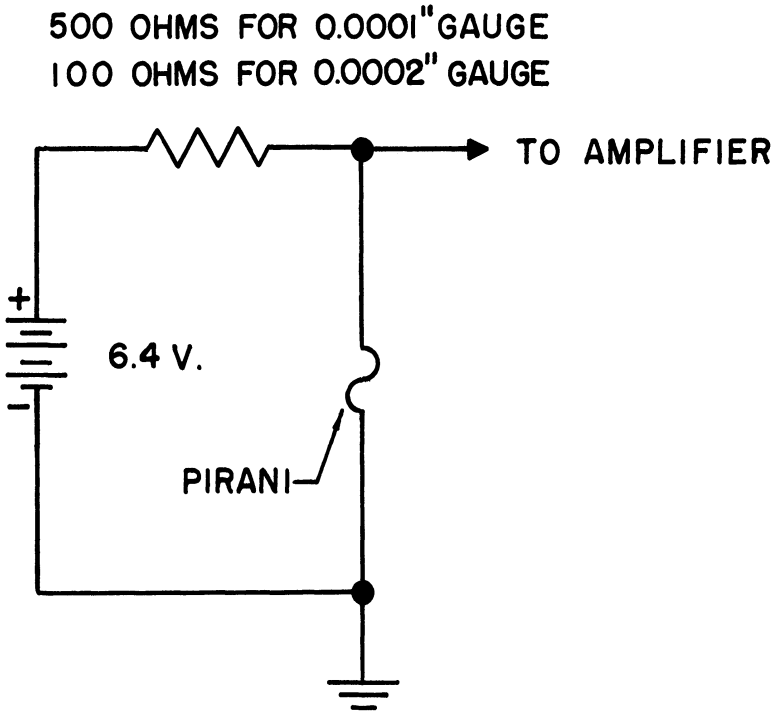

FIGURE 20 PIRANI GAUGE CIRCUIT

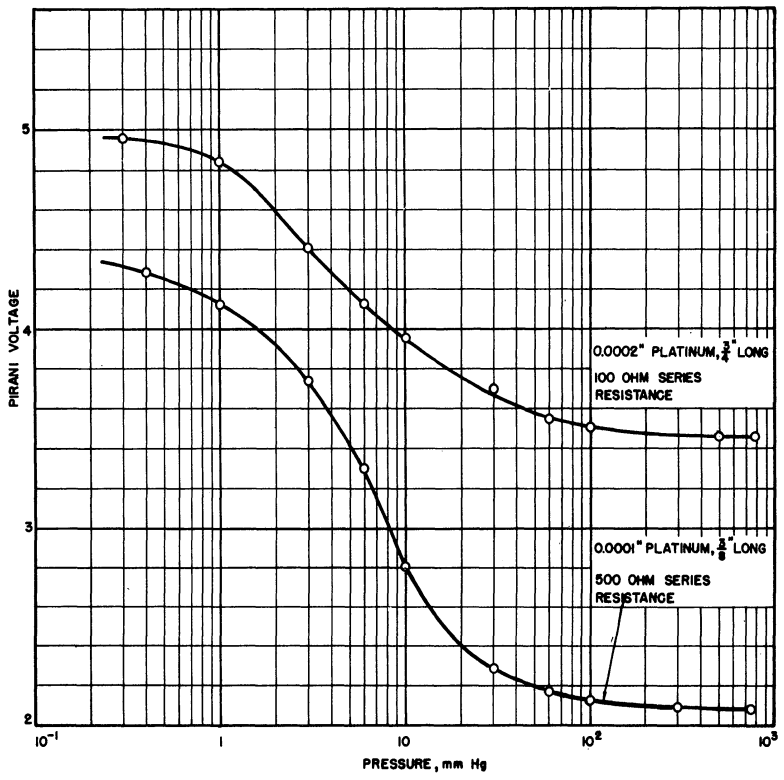

FIGURE 21. STATIC CHARACTERISTIC CURVES OF PIRANI GAUGES

TABLE 2

PIRANI GAUGE SIGNALS

Altitude 10^3 ft.	V ft./sec.	P_{01}' mm. Hg.	P_{ow}' mm. Hg.	Pirani Signal peak input volts		Amplified Pirani Signal predicted peak volts		Amplified Pirani Signal obtained on V-2 #56 peak volts	
				0.0001"	0.0002"	0.0001"	0.0002"	0.0001"	0.0002"
98.2	4360	186.0	309.0	.015	.013	0.60	0.52	1.00	1.05
131.5	4180	35.6	66.0	.084	.080	1.68	1.60	1.05	0.70
164.2	3839	9.1	14.1	.320	.138	2.88	2.07	0.95	0.82
196.9	3550	2.47	3.63	.190	.172	2.47	2.24	1.75	0.93
229.7	3248	0.447	0.637	.062	.025	1.24	0.70	0.35	0.58

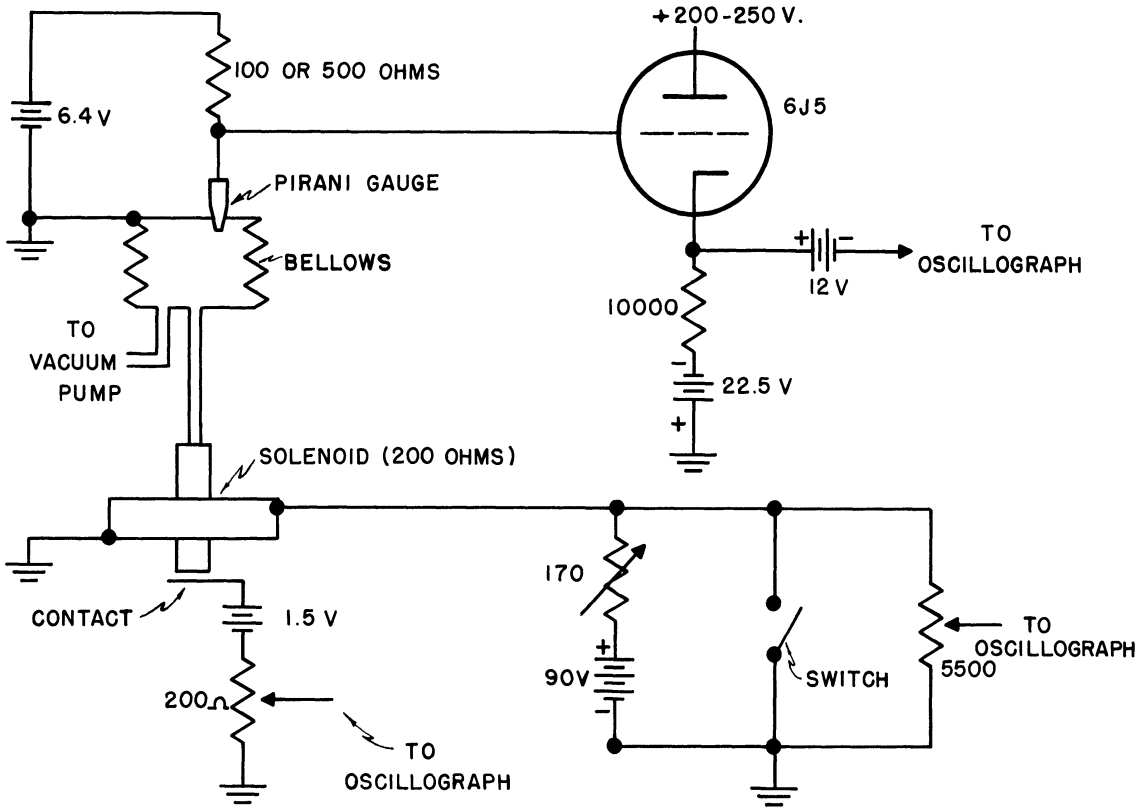

FIGURE 22. "MECHANICAL METHOD" OF MEASURING PIRANI TIME CONSTANTS.

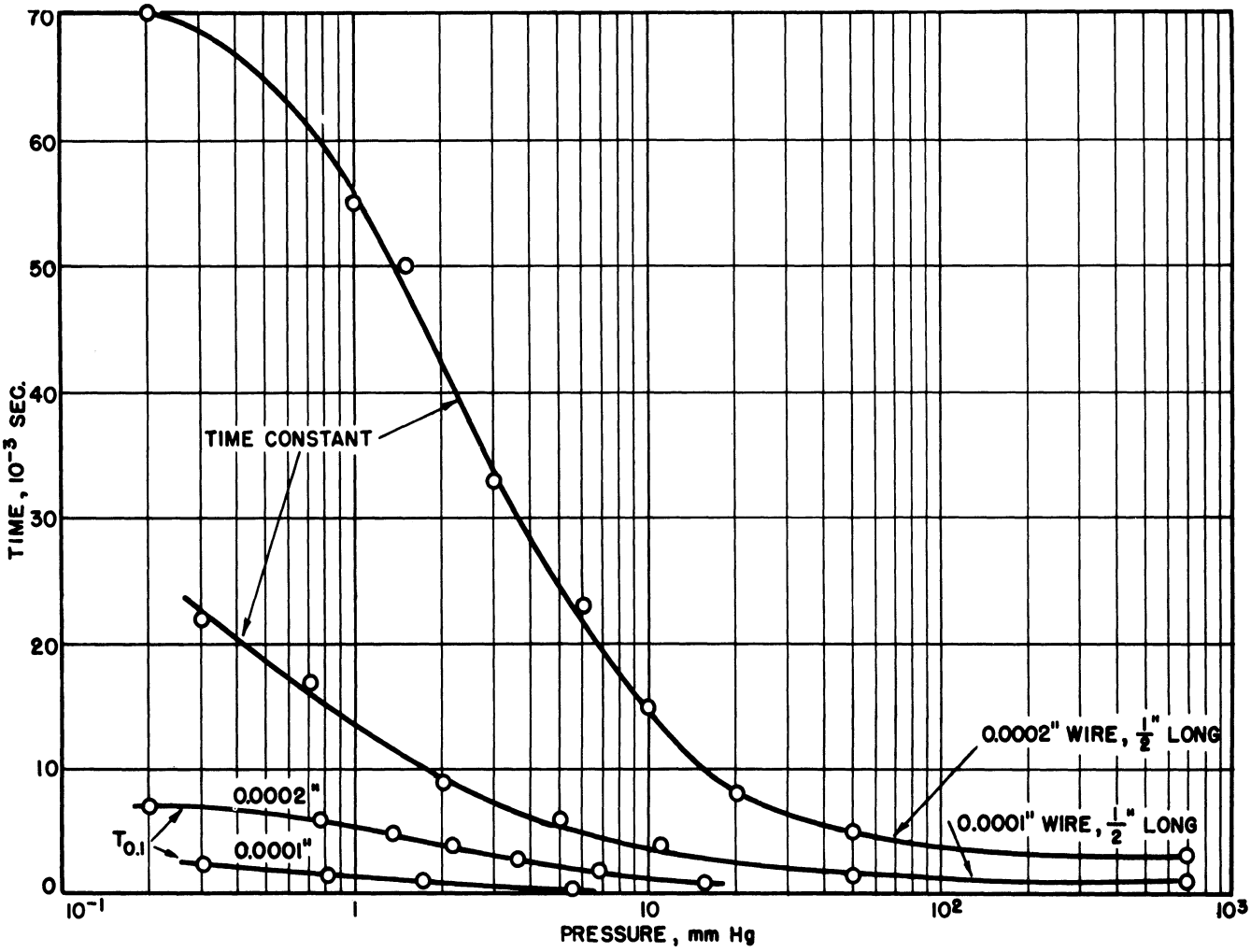

FIGURE 23. PIRANI GAUGE TIME CONSTANTS

The time constant of one of these gauges would be slightly less than that of a 0.5 inch gauge. The 0.0001" diameter wires were .375 inches long; the time constant of one of these would be somewhat greater than that of a 0.5 inch gauge. It is believed that the true values of time constants of the Pirani gauges used on V-2 number 56 lie in the range indicated by figure 23.

The accuracy of determination of the position of the probe at the instant it intersects the shock wave depends upon the time constants of the gauges used. We assume that the accuracy of signal determination corresponds to the time ($T_{0.1}$) required for the Pirani gauge signal to complete one-tenth of its total change. The probable range of values of $T_{0.1}$ for the gauges used on V-2 number 56 are also shown in figure 23.

5.3 Pirani Amplifier and Other Instrumentation

The schematic diagram of the amplifier used on V-2 Number 56 is shown in figure 24. The amplifier gain was made to depend upon the amplitude of the signal input by inserting a non-linear resistance (thyrite) in the grid circuit of the output stage. The gain was greater for small signals than for large signals. The characteristic curves of the amplifier are shown in figure 25. The gain of the amplifier was made to drop-off rapidly at frequencies greater than 600 cycles in order to discriminate against high frequency noise components while still permitting the accurate determination of the time at which Pirani signals occurred. The magnitude of the amplified expected Pirani signals are shown in Table 2.

Data were recorded on two systems. The primary unit was the Naval Research Laboratory Pulse Matrix Telemetering system. The secondary unit which was flown to insure that data would be obtained, was a Cook Research Laboratories 13 channel magnetic tape recorder. The unamplified signals of each probe were recorded on one channel in each system. The amplified signals of each probe were recorded on two telemeter channels and on one Cook recorder channel. The probe position was recorded on two channels in each system.

The probe position was recorded as follows. Phosphor bronze wiper arms attached to each probe rod made electrical contact at five calibrated points along the length of travel of the probe. The signals obtained were applied directly to the recording systems.

DOVAP (doppler velocity and position instrumentation) provides the most accurate determination of velocity. However, because of interference with the telemetering system, it was not used on V-2 Number 56. The askania camera velocity and position data were used for temperature calculations. Mitchell Theodolite and radar velocity and position data were also obtained.

Rocket attitude data were obtained by tracking telescopes and the modified K-25 camera flown by APL on this missile.

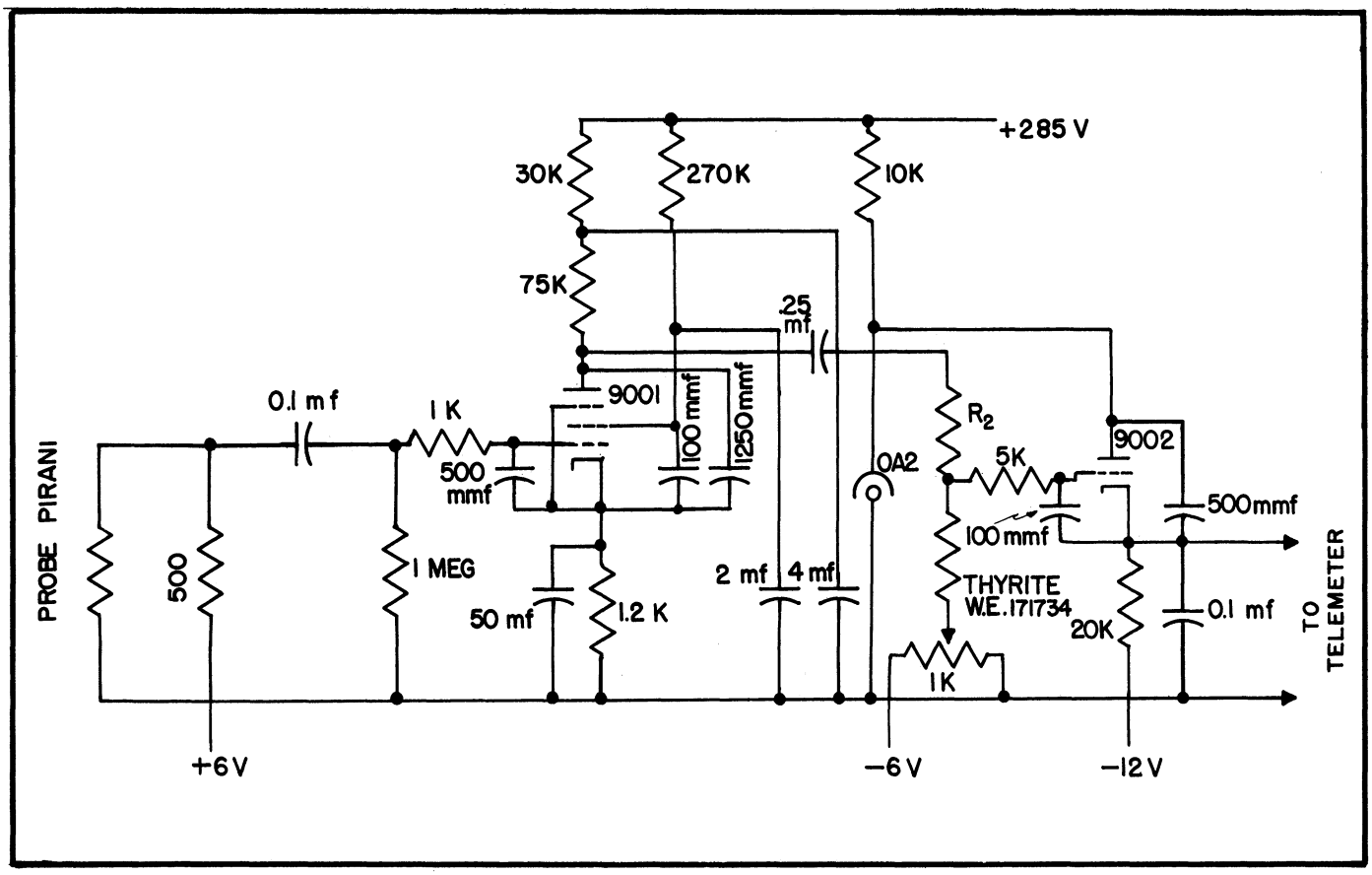

FIGURE 24 SCHEMATIC DIAGRAM OF AMPLIFIER USED ON V-2 NUMBER 56

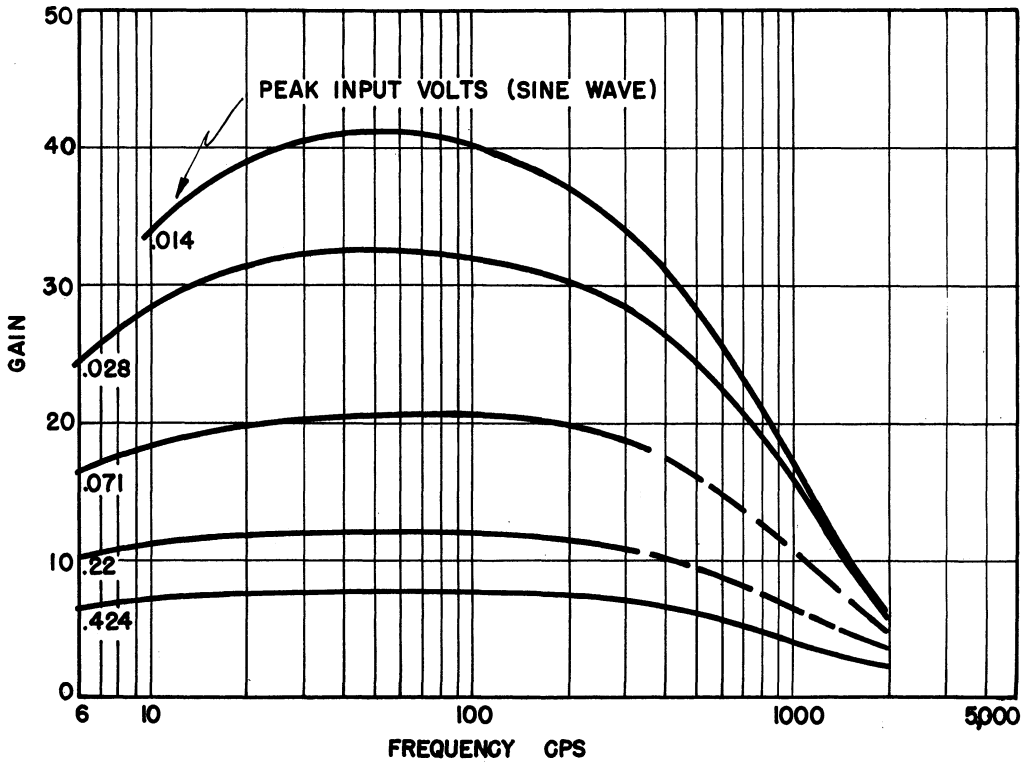

FIGURE 25 CHARACTERISTIC CURVES OF V-2 NUMBER 56 AMPLIFIER

6. CALIBRATION OF THE EXPERIMENT

6.1 The Nose Cone

Because the included angle of the shock wave cone depends critically upon the apex angle of the nose cone of the rocket, it was necessary to have the nose cone machined very accurately. After machining, the diameter of the cone was measured at one inch intervals for 16 inches back from the tip of the cone. The measurements showed that the top two inches of the cone curved in slightly from a true conical surface. It is not known what effect this curved tip had on the position of the shock wave 12 to 16 inches back from the cone tip (all data on V-2 Number 56 were obtained in this region) however, it is assumed to be small.

For the purpose of calculating the shock wave angle, a conical surface was fitted to the measured values of cone diameter in the following manner (see Figure 26). The method of least squares was used to calculate the coefficients for the line:

$$x = a + bZ \tag{9}$$

In which Z was the distance back from the cone tip and x the radius of the cone at this distance back from the tip. It was assumed that the probable error in the measured values of x_i was much greater than the probable error in the measured values of Z_i (R16). The results are shown in Table 3. Comparison of measured diameters with the corresponding fitted values show excellent agreement.

6.2 The Probes

It has been noted that the motion of each probe was measured by electrical signals obtained at five calibrated points. The calibration was made in the following manner. The probes were moved by manually turning the drive shaft. Starting with the probes in their lowest position, the probe was moved slowly up to the first point at which the wiper arm made electrical contact. This was indicated by the lighting of a lamp connected into the signal circuit. The distance from the top surface of a carefully ground cross bar to the top of the probe rod was then carefully measured with a depth gauge as shown in Figure 27. The distance from the tip of the probe to the tip of the nose cone was calculated from the relation:

$$z = z_o + z_a - z_c + z_d + z_f - z_g \tag{10}$$

where the auxiliary dimensions are as shown in Figure 27. These auxiliary dimensions were measured with micrometer type gauges.

TABLE 3

RESULTS OF LEAST SQUARES ADJUSTMENT OF CONICAL ROCKET TIP DATA

$x = a + bz$

$a = 0.0152 \pm 0.0045$

$b = 0.3646 \pm 3 \times 10^{-6}$

$\theta_s = \arctan b = 20.03^\circ \pm 0.0001^\circ$

Measured Values	z_i	.0417*	1	2	3	4	5	6	7	8
	x_i	0	0.3770	0.7450	1.1105	1.4725	1.8380	2.2018	2.5655	2.9330
Fitted Values	x	0	0.3798	0.7444	1.1089	1.4735	1.8381	2.2027	2.5673	2.9319

Measured Values	z_i	9	10	11	12	13	14	15	16
	x_i	3.2970	3.6640	4.0280	4.3935	4.7555	5.1190	5.4800	5.8465
Fitted Values	x	3.2964	3.6610	4.0256	4.3902	4.7548	5.1194	5.4839	5.8485

*Fitted Value of z_o

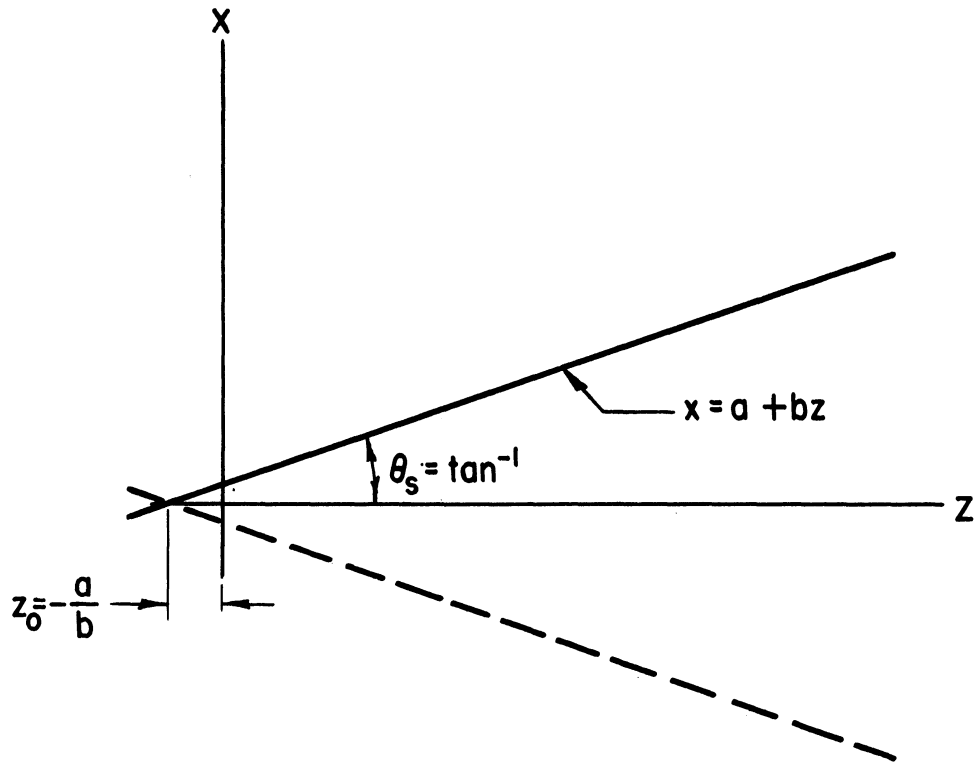

FIGURE 26. METHOD OF FITTING CONICAL SURFACE TO NOSE CONE USED ON V-2 NUMBER 56.

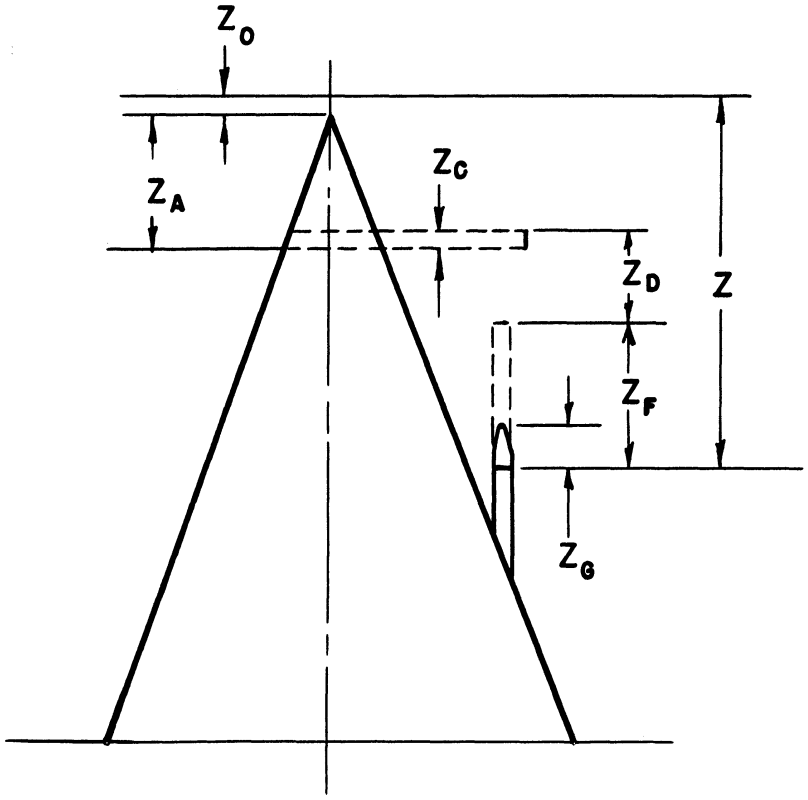

FIGURE 27. CALIBRATION OF LONGITUDINAL DISTANCE OF PROBE.

Each signal point on the cycle of each probe was calibrated in this manner. The results are shown in Table 4.

The lateral distance from the center line of the cone to the center of the probe was measured as indicated in Figure 28. X_0, the lateral distance for the probe at the lower end of its travel was taken to be one-half of the center distance of diametrically opposite probes. The lateral distance at the upper end of the travel X_1 was obtained from:

$$X_1 = \frac{d_1}{2} + S_2 + \frac{d_2}{2} \tag{11}$$

where the distances involved are as shown in the Figure.

Lateral distances corresponding to a given vertical distance from the tip were calculated on the assumption that the probe traveled in a straight line between these two points. Thus the lateral distance for a point at a distance z from the cone tip was obtained from the relation:

$$X = X_0 + \frac{(z_1 - z)}{(z_1 - z_0)} (X_1 - X_0) \tag{12}$$

where z_0 and z_1 are the vertical distances from the cone tip to the probe tip at the lower and upper ends of probe travel, respectively.

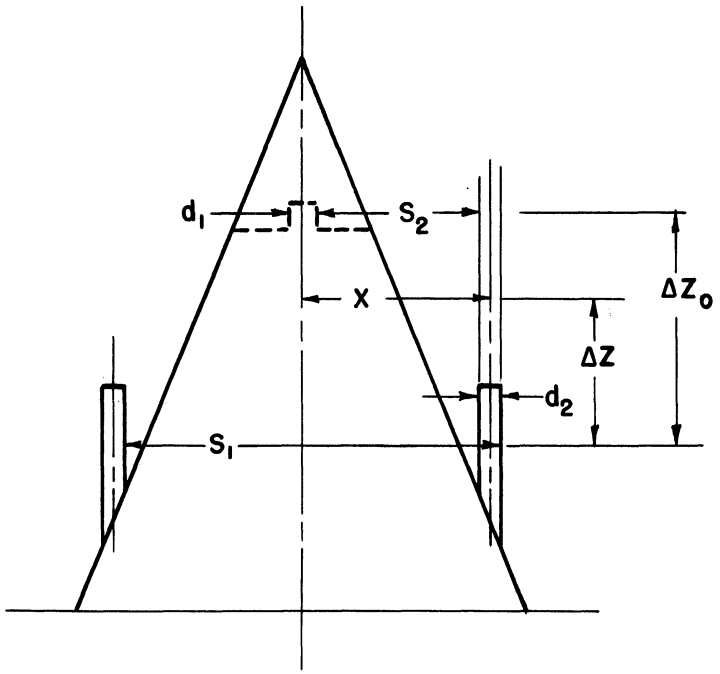

FIGURE 28. CALIBRATION OF LATERAL DISTANCE OF PROBE.

TABLE 4

PROBE CALIBRATION DATA

Probes Ascending: ↑ Probes Descending: ↓

Commutator Positions	z - Coordinate			
	Probe 1	Probe 2	Probe 3	Probe 4
1 ↑	-17.198	-16.900	-16.444	-16.064
2 ↑	-15.625	-15.319	-14.864	-14.489
3 ↑	-14.054	-13.740	-13.284	-12.908
4 ↑	-12.473	-12.159	-11.716	-11.325
5 ↑	-10.888	-10.585	-10.131	- 9.748
5 ↓	-10.761	-10.433	- 9.980	- 9.628
4 ↓	-12.331	-12.007	-11.555	-11.207
3 ↓	-13.908	-13.588	-13.147	-12.783
2 ↓	-15.495	-15.167	-14.719	-14.362
1 ↓	-17.069	-16.742	-16.297	-15.942

7. DISCUSSION OF THE CALCULATIONS

7.1 Probe Position

The excellent telemeter records obtained on the flight contained the following information necessary to the calculation of upper atmosphere ambient temperatures: a record of probe position against time, and a record of shock wave signals against time. A sample of the telemeter record is shown in Figure 29. The vertical dotted lines are half-second timing markers. This is the zero time base used as a standard of reference for all data obtained on the flight. The amplified probe signals are shown in channels 1, 2, 4, 5; the probe position signals are in channel 3.

The amplitudes of some of the signals obtained are shown in Table 2 for comparison with the expected signals. At low altitudes the signals obtained were of larger amplitude than expected as illustrated by the signal at 60,900 feet. Above 153,000 feet the signals obtained were smaller than expected. The signals at low altitudes also differed in pattern from what was expected, whereas the pattern of signals at high altitudes was as expected. The patterns of signals obtained are shown in Figure 30. This evidence indicates that the method used to predict shock wave signals (Section 5.2) is valid only qualitatively. The above data can be used, however, as an empirical guide in predicting signals for future rocket flights.

A graph of probe position (distance from tip of nose cone) against time was plotted for each half cycle of each probe. The time of a given probe position signal was obtained from the telemeter records by interpolating linearly between the nearest one-second time markers, as shown in Figure 31a. The graphs show that the speed of the probes was essentially constant over the entire length of probe travel.

The time of a shock wave signal was obtained from the telemeter record by the same interpolation method (see Figure 31b). The probe position corresponding to a shock wave signal was obtained from the graphs of probe position against time. The lateral distance for each signal was obtained from the formula (12) of Section 6. The data is given in Table 5. The co-ordinate system used is explained in Section 7.3.

7.2 The Shock Cone is Assumed to be a Right Circular Cone

In the following calculations the shock wave is assumed to be a right circular cone. In Section 2 it was stated that this is approximately true for angles of yaw less than two degrees. Figure 32 contains a plot of rocket yaw (the angle between the rocket trajectory and missile axis) obtained from the APL modified K-25 camera. We are actually interested in the angle ϵ between the nose cone axis and the free stream velocity vector of the air. In order to obtain this angle ϵ, it is necessary to correct the observed yaw

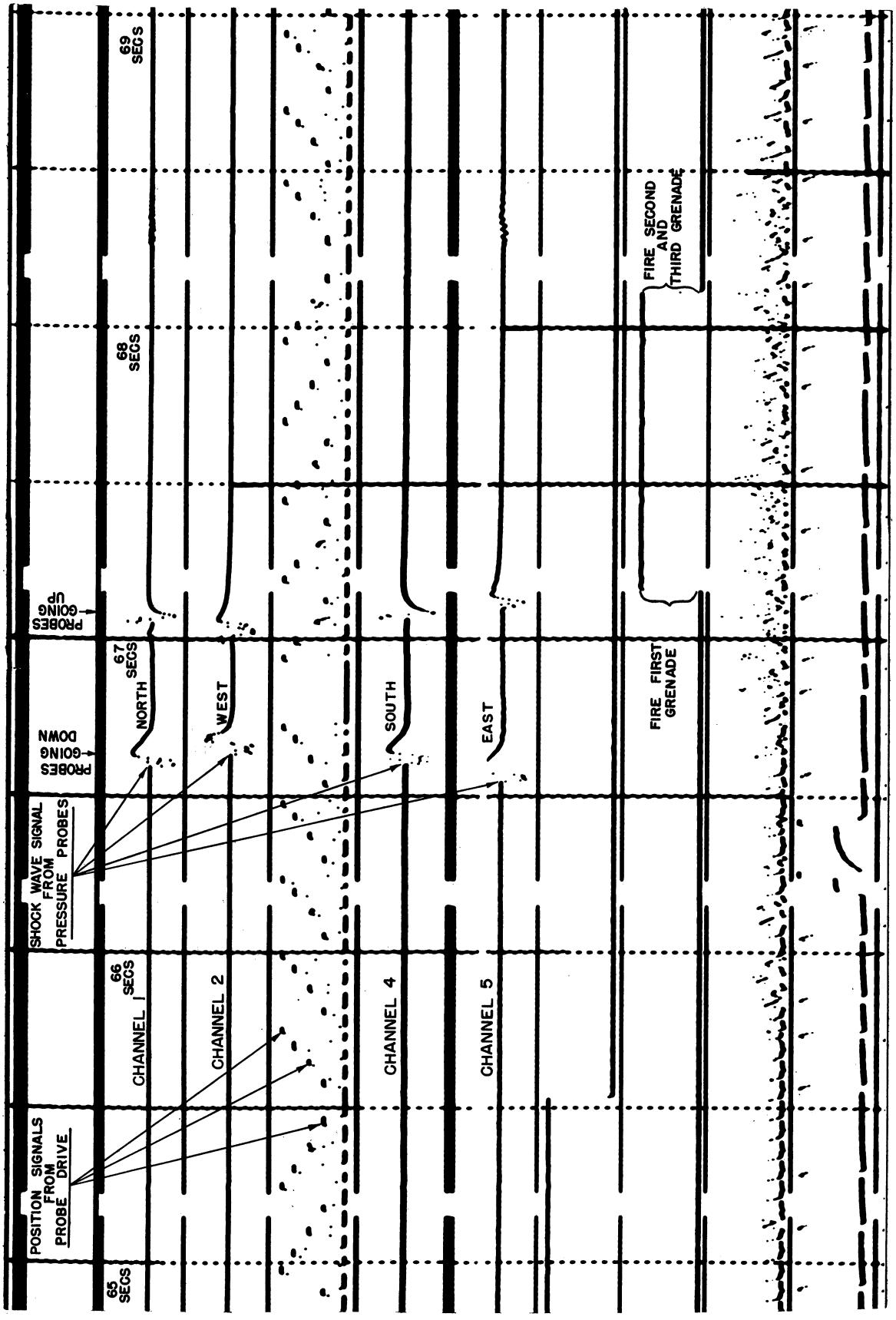

FIGURE 29. PORTION OF TELEMETER RECORD OBTAINED ON V-2 NUMBER 56.

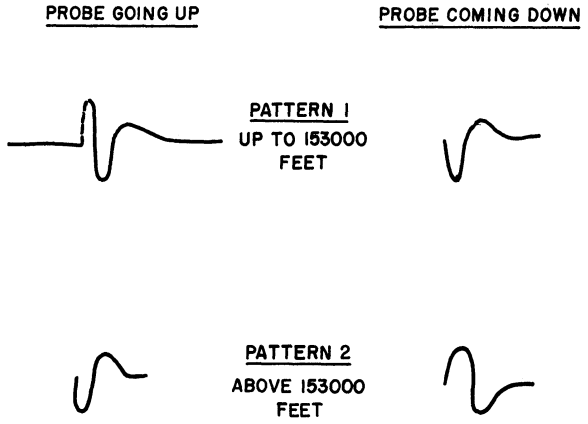

FIGURE 30 PATTERNS OF SIGNALS OBTAINED ON V-2 NUMBER 56

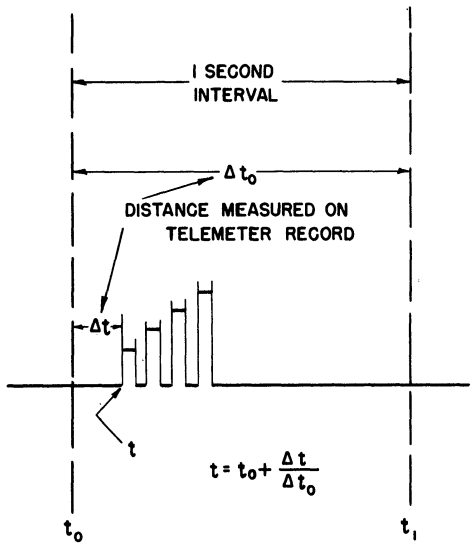

FIGURE 31a. METHOD OF DETERMINING THE TIME OF OF A PROBE POSITION SIGNAL.

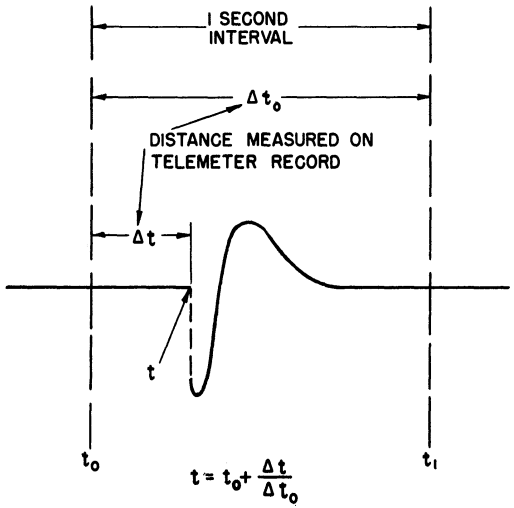

FIGURE 31b. METHOD OF DETERMINING THE TIME OF A SHOCK WAVE SIGNAL.

TABLE 5

MEASURED COORDINATES[1] OF POINTS ON SURFACE OF SHOCK CONE

Cycle	Probe 1				Probe 2				Probe 3				Probe 4			
	Time[2]	x	y	z	Time[2]	x	y	z	Time[2]	x	y	z	Time[2]	x	y	z
1 ↑	58.048	8.057	0	-15.381	58.035	0	8.056	-15.449	58.059	-8.053	0	-15.251	58.072	0	-8.051	-15.253
1 ↓	60.226	7.962	0	-15.819	60.243	0	7.961	-15.851	60.218	-7.958	0	-15.636	60.191	0	-7.957	-15.601
2 ↑	60.907	8.056	0	-15.918	60.887	0	8.054	-16.001	60.907	-8.052	0	-15.868	60.936	0	-8.051	-15.775
2 ↓	63.298	7.960	0	-16.241	63.326	0	7.959	-16.386	63.292	-7.958	0	-16.131	63.256	0	-7.957	-15.991
3 ↑	63.797	8.054	0	-16.361	63.777	0	8.053	-16.476	63.808	-8.051	0	-16.298	63.837	0	-8.051	-16.141
3 ↓	66.092	7.960	0	-16.336	66.131	0	7.959	-16.499	66.098	-7.957	0	-16.271	66.043	0	-7.957	-16.034
4 ↑	66.548	8.054	0	-16.441	66.506	0	8.052	-16.731	66.561	-8.051	0	-16.336	66.598	0	-8.051	-16.156
4 ↓	68.751	7.961	0	-15.971	68.775	0	7.960	-16.098	68.797	-7.957	0	-16.181	68.767	0	-7.957	-16.121
5 ↑	69.317	8.055	0	-15.991	69.299	0	8.054	-16.116	69.272	-8.051	0	-16.251	69.297	0	-8.051	-16.139
5 ↓	71.378	7.963	0	-15.630	71.446	0	7.960	-16.000					71.386	0	-7.957	-15.700
6 ↑	72.078	8.057	0	-15.490	72.014	0	8.055	-15.895					72.066	0	-8.051	-15.595
6 ↓	74.084	7.963	0	-15.490	74.152	0	7.961	-15.883					74.062	0	-7.957	-15.360
7 ↑	74.802	8.057	0	-15.500	74.763	0	8.055	-15.753					74.847	0	-8.051	-15.265
7 ↓	76.832	7.963	0	-15.511									76.807	0	-7.957	-15.373
8 ↑	77.577	8.057	0	-15.440									77.572	0	-8.051	-15.507
8 ↓	79.593	7.964	0	-15.100									79.630	0	-7.957	-15.348
9 ↑	80.493	8.059	0	-14.998									80.424	0	-8.051	-15.433
9 ↓	82.306	7.968	0	-14.205									82.398	0	-7.957	-14.814

1) Coordinate system of Figure 34

2) Time after Take-off.

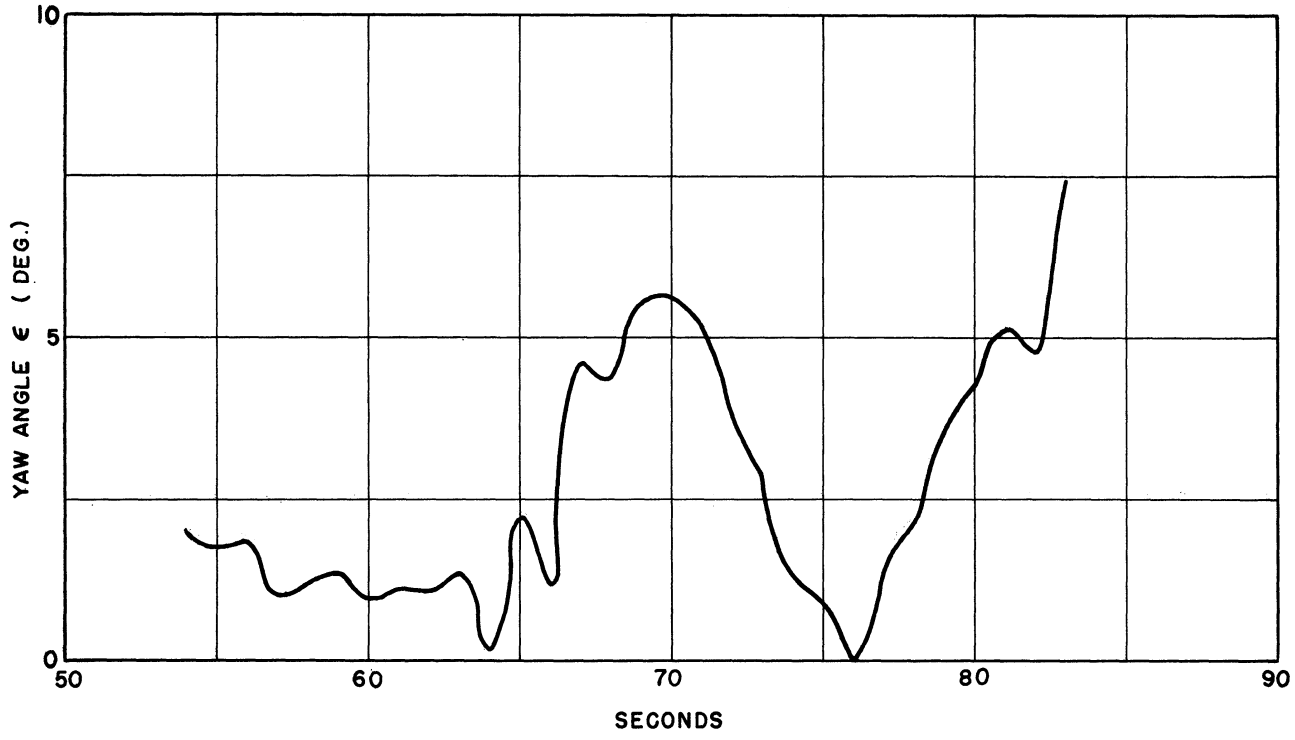

FIGURE 32, ROCKET YAW

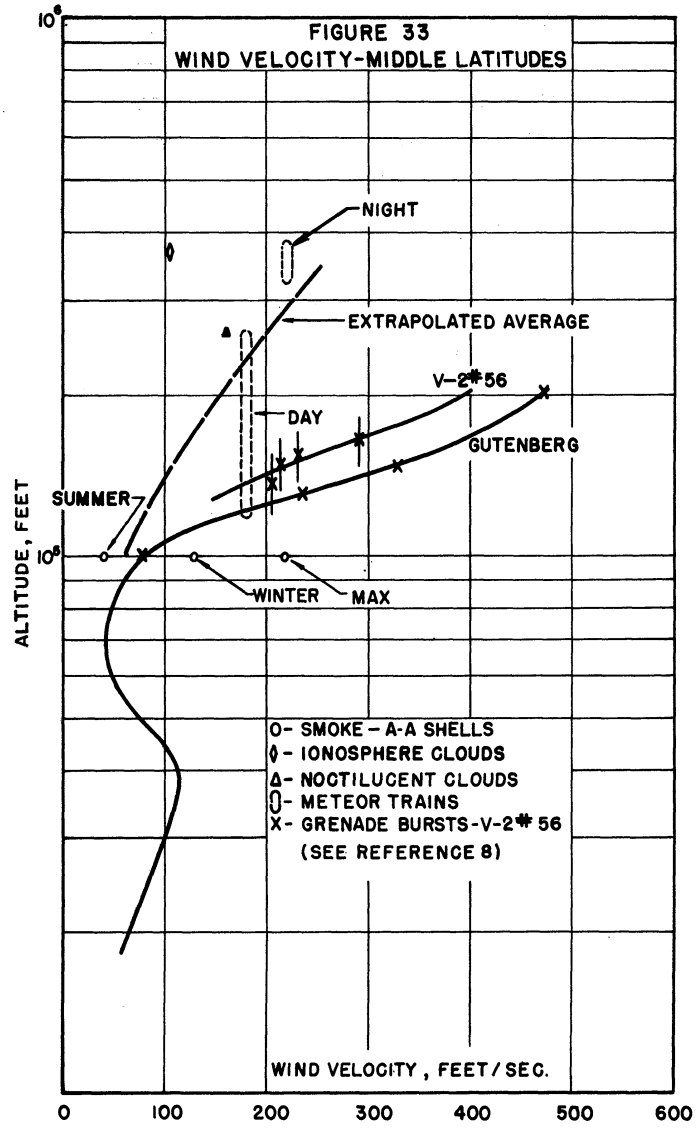

Fig. 33

Wind Velocity - Middle Latitudes

data for winds. Some wind data were obtained from the bursts of four grenades ejected from the missile during flight. (R17). These wind data are plotted in figure 33 along with an average wind velocity curve for middle latitudes based on other kinds of observations. (R8). The APL attitude data have been corrected for wind velocities in the range of 70-83 seconds (134,000 to 184,000 feet). In doing this it was assumed that the direction in which the wind was blowing was due east. The calculations are shown in Table 6. The angle ϵ is small except after 67 seconds (121,000 feet). The amount by which the shock cone varies from the true right circular cone was shown in Section 3.2, Table 1. This effect has been neglected in the calculations.

7.3 Equation of the Shock Cone

The general equation of a right circular cone in terms of a rectangular cartesian coordinate system x, y, z with origin at the cone tip (see figure 34) can be written as:

$$x^2 + 2bxy + cy^2 + 2dxz + 2eyz + fz^2 = 0 \tag{13}$$

If the z axis of the coordinate system coincides with the longitudinal axis of the cone (no yaw) this equation reduces to the relation:

$$x^2 + y^2 + fz^2 = 0 \tag{14}$$

in which the tangent of the semi apex angle of the cone is:

$$\tan \theta_W = \sqrt{-f} \tag{15}$$

Thus, in the non-yawed case, we can calculate θ_W if we measure the coordinates of one point on the cone surface. The general case, equation (13), can also be written as:

$$xA + yB + zC + \sqrt{x^2 + y^2 + z^2} = 0 \tag{16}$$

with

$$\begin{aligned} A &= \sin \phi \sin \xi \sec \theta_W \\ B &= \sin \phi \cos \xi \sec \theta_W \\ C &= \cos \phi \sec \theta_W \\ \sec \theta_W &= \sqrt{A^2 + B^2 + C^2} \end{aligned} \tag{17}$$

$$\phi = \epsilon - \delta = \epsilon (1 - \alpha) \tag{18}$$

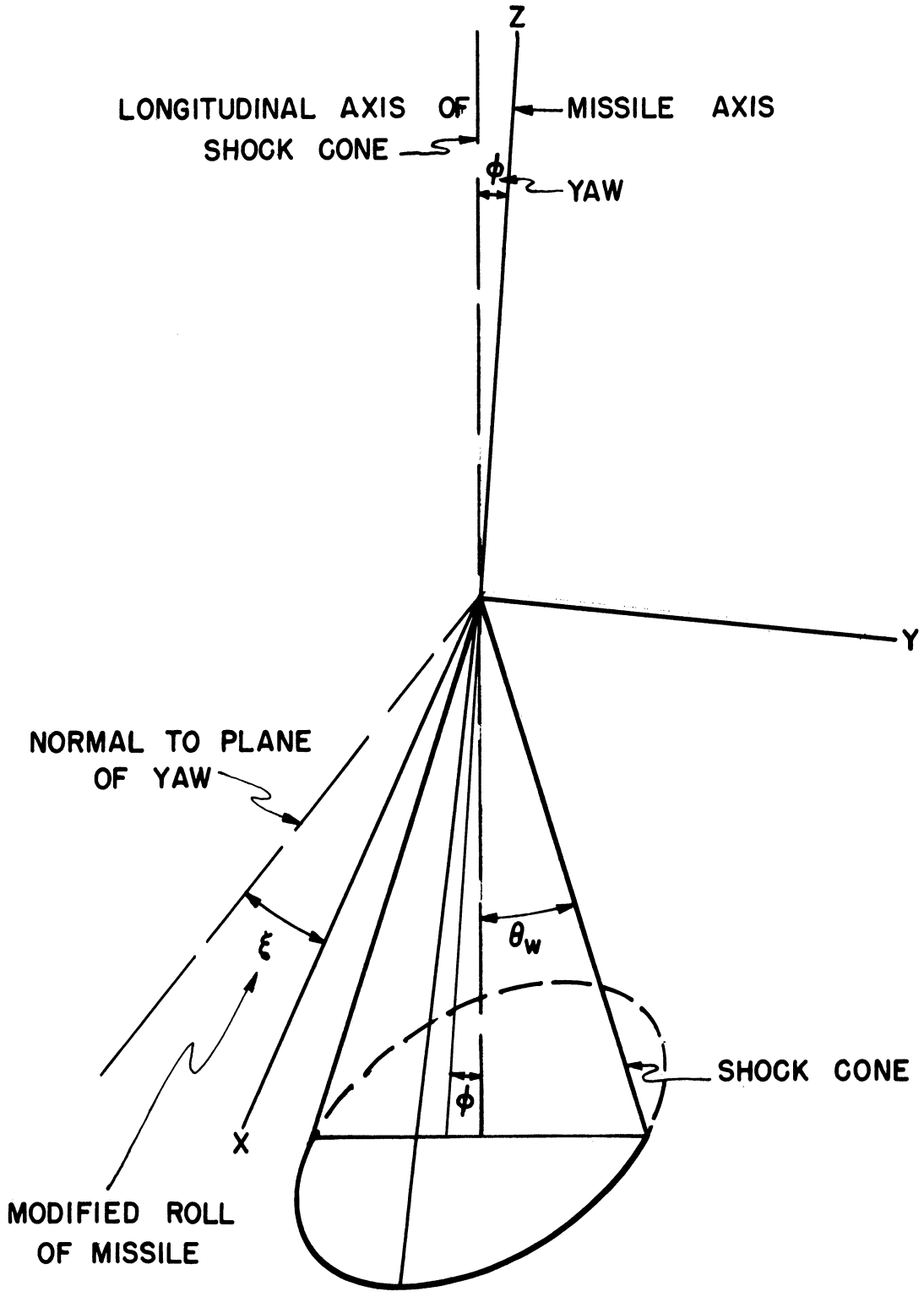

FIGURE 34

RIGHT CIRCULAR CONE YAWED WITH RESPECT TO COORDINATE SYSTEM

TABLE 6

V-2 NUMBER 56 YAW DATA

Time (secs.)	Altitude (10^3 ft.)	Vx	Vy	Vw	Vy'	Vz	V	Cos α_1	Cos α_2	Cos α_3	Cos β_1	Cos β_2	Cos β_3	Cos ϵ	$P_{\cos\epsilon}$	ϵ	P_ϵ
		ft./sec.															
54	72.5	379	33			3034	3058	.12393	.01079	.99215	.15454	.01780	.98782	.99941		1.97°	
55	75.5	400	38			3114	3140	.12738	.01210	.99171	.15160	.02757	.98806	.99952		1.77°	
56	78.7	420	37			3242	3270	.12844	.01131	.99143	.15799	.00960	.98752	.99946		1.88°	
57	81.9	434	37			3330	3358	.12924	.01101	.99166	.15195	.01117	.98833	.99985		1.00°	
58	85.3	452	36			3441	3470	.13025	.01037	.99164	.15902	.00890	.98725	.99980		1.15°	
59	88.8	471	35			3560	3591	.13116	.00974	.99136	.15246	.02094	.98805	.99971		1.37°	
60	92.4	493	34			3688	3721	.13249	.00913	.99113	.13347	.00733	.99103	.99986		0.95°	
61	96.2	515	32			3821	3855	.13359	.00830	.99118	.15833	.01797	.98722	.99981		1.12°	
62	100.1	534	31			3940	3976	.13430	.00779	.99094	.15557	.01396	.98779	.99984		1.08°	
63	104.1	548	31			4038	4075	.13447	.00760	.99092	.15040	.02600	.98828	.99973	± .0070	1.33°	±17°
64	108.2	562	30			4116	4154	.13529	.00722	.99085	.14332	.01535	.98955	.99999		0.15°	
65	112.3	576	30			4172	4212	.13675	.00712	.99050	.15351	.04013	.98733	.99923		2.25°	
66	116.5	586	30			4207	4247	.13797	.00706	.99058	.14884	.03193	.98833	.99978		1.20°	
67	120.8	591	31			4205	4246	.13918	.00730	.99034	.18121	.07655	.98044	.99675		4.62°	
68	125.0	591	31			4182	4224	.13991	.00733	.99005	.19064	.06088	.97978	.99715		4.33°	
69	129.1	590	31			4158	4200	.14047	.00738	.99000	.22019	.06053	.97358	.99522		5.61°	
70	133.3	591	31			4148	4190	.14105	.00739	.98997	.23005	.04536	.97213	.99516		5.64°	
71	137.4	595	31	185	216	4138	4186	.14214	.05160	.98853	.23175	.05007	.97151	.99589		5.19	
72	141.6	599	32	200	232	4115	4165	.14381	.05570	.98799	.20962	.05198	.97641	.99772		3.87	
73	145.7	600	33	215	248	4081	4132	.14520	.06001	.98765	.19380	.07498	.97815	.99871		2.91	
74	149.7	599	34	230	264	4049	4101	.14602	.06435	.98707	.15660	.07498	.98481	.99977		1.22	
75	154.3	579	26	242	268	4010	4060	.14261	.06600	.98768	.14125	.08768	.98608	.99986		0.95	
76	158.3	601	32	260	292	4006	4061	.14799	.07190	.98645	.14712	.07080	.98657	1.00007		0	
77	162.3	594	32	277	309	3957	4013	.14801	.07699	.98604	.12117	.08403	.98907	.99967		1.47	
78	166.3	588	34	290	324	3966	4022	.14619	.08055	.98607	.11182	.10036	.98866	.99932		2.12°	
79	170.2	599	33	310	343	3931	3991	.15008	.08594	.98496	.09845	.12222	.98761	.99804		3.58°	
80	174.1	587	33	322	355	3840	3901	.15047	.09100	.98436	.08525	.12585	.98839	.99721	± .0082	4.28°	± 6°
81	177.9	586	21	337	358	3773	3835	.15280	.09335	.98383	.08577	.15161	.98470	.99604		5.10°	
82	181.5	590	31	347	378	3774	3838	.15372	.09848	.98332	.10349	.16575	.98068	.99655		4.77	
83	185.2	593	32	357	389	3723	3790	.15646	.10263	.98232	.06802	.19680	.97808	.99163		7.42	

where

ϕ = the angle of yaw between the cone axis and the z axis of the co-ordinate system.

ξ = the azimuth angle between the normal to the plane of yaw and the x axis of the coordinate system.

θ_w = the semi apex angle of the cone.

If we measure the co-ordinates of three points on the cone surface, we can solve for A, B, C in equation (16), and for θ_w using equation (17).

7.4 Calculation of the Shock Cone Angle

On V-2 number 56, data were obtained from four probes during the period 58 to 72 seconds; from three probes in the range 72 to 75 seconds; and from two probes between 75 and 96 seconds. After 96 seconds, Pirani gauge signals were not clear enough for accurate determination of the corresponding probe position. The details of shock angle calculations are covered in the next three sections.

7.41 Four Probe Data

During this period of time, we have independent measurements of four points on the surface of the cone for each encounter of the probes with the shock wave. Figure 32 shows that the yaw (ϵ) was small; the angle ϕ , approximately 0.2 ϵ is also small. Therefore as an initial calculation, four values of θ_w were calculated for each set of data using equations (14) and (15) which apply in the non-yawed case. The average of the four angles was found. The data are shown in Table 7. The results of this calculation confirmed the fact that yaw is small, for the individual values of θ_w in each set agree fairly well.

Since the coordinates of three points on the surface of the cone and equations (16) and (17) will determine the shock cone uniquely, the calculations were next made in this way. There are four combinations of four things taken three at a time. A calculation was made for each of the four combinations and an average was then found. These data are also shown in Table 7. The average values are almost identical with the values obtained by the first method.

Since we have more than the minimum data needed to calculate the shock angle, the data can be adjusted statistically using the method of least squares (R16). Starting with approximate values of A, B, C and the (experimental) values of the coordinates of the four points, we find adjusted values of A, B, C and the coordinates such that the square root of the sum of the squares of the residuals of the

coordinates is a minimum. This was done for several points. The θ_w obtained in this way for these points was the same as that obtained by the other calculations. It is assumed that the results would be the same for all of the four probe data. This will be checked at the first opportunity.

7.42 Three Probe Data

Independent measurements of three points on the cone's surface were obtained. Yaw was larger than for the period of four probe data. Calculations were made by the second method described in Section 7.41 (using equations (16) and (17)). The results are shown in Table 7.

7.43 Two Probe Data

Independent measurements of only two points on the cone's surface were obtained during this period. Yaw was large so that the first method (Section 7.41) could not be used. The second method (Section 7.42) requires the coordinates of three points on the cone's surface. Thus additional data were needed for the calculation of shock angle in this region.

Missile attitude data were obtained from the APL K-25 camera film (R22). These were used with askania trajectory data (R18) and the wind velocity data to compute yaw ϵ and the azimuth angle ξ Although these data had fairly large probable errors they were used with the probe data to calculate shock angles by the method 3 of Section 7.41. The approximate values of A, B, C needed for this statistical adjustment were obtained as follows.

A Mach number was assumed; the factor α was obtained from R13, ϕ was calculated from equation (18). ϕ , ξ , and the coordinates of one point on the cone surface were used to calculate A, B, C from equation (16). Another set of values of A, B, C were obtained from equation (16) using ϕ , ξ , and the coordinates of the second point. The averages of these two sets of values were used as the approximate values of A, B, C. In these calculations it was necessary to find by successive approximations the proper value of Mach number to use.

The results of this calculation of θ_w by the least squares method are also shown in Table 7. Missile attitude was not available in the time range of 83 to 96 seconds. The APL camera was pointing at the sky during this time and tracking telescopes also failed to provide attitude data during this period. Thus θ_w was calculated from two probe data only up to 83 seconds (183,000 feet) although signals were obtained from two probes up to 96 seconds (230,000 feet).

7.5 Calculation of Temperature

The free stream Mach number corresponding to each of the shock angles θ_w of Table 7 were obtained from R12. The corresponding ambient air temperatures were then calculated from the relation for

TABLE 7

SHOCK ANGLE, MACH NUMBER, AND CALCULATED AMBIENT TEMPERATURES

Cycle up ↑ down ↓	Altitude 10^3 ft. above sea level	Time sec.	θ_w^o Method 1					θ_w^o Method 2					θ_w^o Method 3	Mach No.	Speed of Missile ft./sec.	Temp. Deg. Kelvin
			1	2	3	4	Avg.	1,2,3	1,4,3	2,3,4	2,1,4	Avg.				
1 ↑	85.3	58.054	27.65	27.54	27.84	27.83	27.72	27.74	27.74	27.68	27.68	27.71	27.71	3.519	3477	225° ±2°
1 ↓	93.2	60.220	26.72	26.67	26.98	27.02	26.85	26.84	26.85	26.84	26.84	26.84		3.849	3750	219
2 ↑	95.8	60.909	26.85	26.72	26.91	27.04	26.88	26.88	26.88	26.87	26.89	26.88		3.832	3843	232
2 ↓	105.3	63.293	26.11	25.91	26.26	26.46	26.18	26.19	26.19	26.18	26.18	26.18		4.164	4098	223
3 ↑	107.4	63.805	26.21	26.05	26.29	26.51	26.24	26.25	26.25	26.30	26.28	26.27		4.115	4139	233
3 ↓	116.9	66.091	25.98	25.75	25.95	26.39	26.02	26.03	26.02	26.07	26.07	26.05		4.227	4247	233
4 ↑	118.9	66.553	26.10	25.70	26.23	26.48	26.13	26.17	26.16	26.09	26.09	26.13		4.191	4246	236
4 ↓	128.2	68.772	26.49	26.31	26.18	26.26	26.31	26.34	26.34	26.29	26.29	26.31		4.094	4205	243
5 ↑	130.3	69.296	26.73	26.55	26.35	26.51	26.53	26.54	26.54	26.53	26.53	26.53		3.988	4197	255 ±4°
5 ↓	139.1	71.416	27.00	26.45	-	26.88	26.66				26.70			3.910	4173	262
6 ↑	141.8	72.040	27.48	26.87	-	27.31	27.09				27.02			3.773	4157	280
6 ↓	150.1	74.107	27.21	26.62	-	27.39	27.00				27.04			3.765	4090	272
7 ↑	152.8	74.774	27.46	27.08	-	27.80	27.45				27.43			3.618	4075	292
7 ↓	161.6	76.820											27.11	3.737	4017	266
8 ↑	164.6	77.575											27.71	3.519	3988	296
8 ↓	172.6	79.611											27.49	3.596	3894	270
9 ↑	175.9	80.459											27.54	3.577	3888	272 ±6°
9 ↓	182.8	82.352											28.06	3.407	3810	288

the speed of sound in a gas (R19)

$$a^2 = \frac{\gamma R}{m_o} T \tag{19}$$

where

a is the speed of sound.

γ is the ratio of the specific heats of the gas.

R is the absolute gas constant.

m_o is the gram molecular weight of the gas.

T is the temperature of the gas.

this relation can be written as

$$T = \left(\frac{V}{65.9M}\right)^2 \tag{20}$$

in which

T is the ambient temperature of the air, degrees Kelvin.

V is the speed of the missile with respect to the air, feet per second.

M is the free stream Mach number.

The results of the temperature calculations are shown in Table 7 and are plotted against altitude in Figure 35. Also shown in Figure 35 are the NACA "tentative standard temperatures" (R20) and a curve due to Whipple (R21). The experimental points lie consistently below the curves of whipple and NACA. Note that the points marked with a cross (obtained when the probe moved up through the shock wave) are all above those marked with a square (obtained when the probe moved down through the shock wave). This discrepancy has not been resolved as yet.

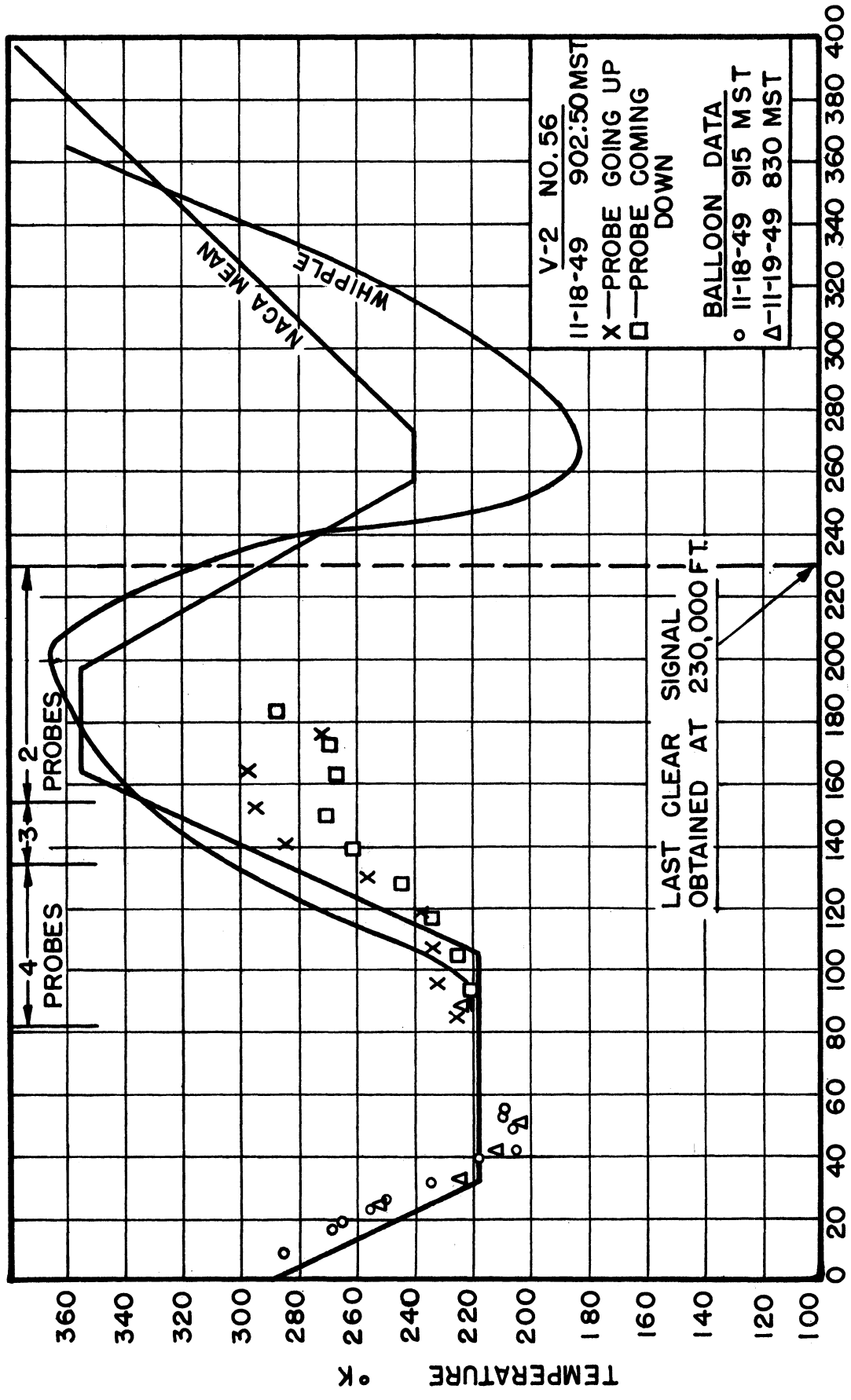

FIGURE 35 AMBIENT TEMPERATURES IN THE UPPER ATMOSPHERE

8. ANALYSIS OF ERROR

8.1 Sources of Error

The sources of error in this method of determining upper air ambient temperatures are conveniently divided into two groups; errors in applying the aerodynamic theory and experimental errors.

8.11 Errors in Applying the Aerodynamic Theory

The second of the five assumptions made in applying Stone's theory, that air is non-viscous, may not be valid at high altitudes, and thus may introduce error. However, the magnitude of the error due to air viscosity cannot be estimated until further tests are made (see Section 10).

The equation of a right circular cone was used in calculating the shock wave angle from the data. This is a first order approximation to the true shock wave shape. The effect of yaw on the shape of the shock cone (according to the second order theory) is shown in Table 1 of Section 3.2. The range of yaw angles and the corresponding possible range of error in the shock angle is given in Table 8. It is to be noted that the yaw data used in these calculations had a large probable error. However, the possible existence of systematic errors as large as shown above must be investigated (see Section 10.)

8.12 Experimental Errors

One of the conclusions of the model test of this experiment was that the Pirani gauge signal was obtained at the moment of the first contact between the tip of the gauge and the shock wave. This conclusion is subject to the possible distortion of the shock wave due to the presence of the probe in the flow field. In the model test, the distortion was shown to be negligible within the accuracy of the experiment which was $\pm 0.5^{\circ}$.

Although the rocket cone was machined accurately, there was some deviation from the true conical shape (Section 6.1). It is not known what effect this had upon the shape of the shock cone in the region measured by the probes, however, it is certain to be small compared to other possible errors.

The error in the coordinates of a point on the surface of the shock cone (corresponding to a given probe signal) had two sources; the process of recording data and subsequently obtaining data from the telemetering records. The relation between the error in coordinate data and the errors of the two sources was obtained by applying the theory of propagation of independent errors to the equations and graphical method which were used to obtain coordinate data from the calibration data and telemetering records.

TABLE 8

POSSIBLE RANGE OF ERROR DUE TO ASSUMPTION THAT SHOCK WAVE IS A RIGHT CIRCULAR CONE

Period	Time Seconds	Yaw Degrees	$\Delta\theta_w$ Degrees
1	58.0 to 69.3	1° to 5.6°	.01° to 0.3°
2	71.4 to 74.8	0° to 5°	0° to 0.3°
3	76.8 to 82.4	1.5° to 7.5°	.02° to 0.8°

TABLE 9

PROBABLE ERRORS BASED ON EXTERNAL CONSISTENCY

Cycle	P_{θ_w}
7 ↓	0.001 Deg.
8 ↑	0.010
8 ↓	0.007
9 ↑	0.019
9 ↓	0.003

TABLE 10

VALUES OF $\frac{\partial M}{\partial \theta_w}$

θ_w	M	$\frac{\partial M}{\partial \theta_w}$	$\frac{\partial M}{\partial \theta_w}\ \frac{1}{M}$
38°	2	.069	.0345
29.7°	3	.233	.0777
26.5°	4	.476	.119

The calibration of probe position was carried out carefully. It is felt that any systematic error in the calibration is negligibly small. An estimate of the probable error in calibration was obtained by making a large number of measurements similar to those made in calibrating the equipment.

The telemetering system had a sampling rate of 312 cycles per second. Thus when a signal was obtained one was certain only that the start of the signal occurred in the previous 3.2 milliseconds. Since this applies to both the shock wave and probe position signals, we can assume that no systematic error is involved but that we have an uncertainty equivalent to a statistical probable error of $\pm$ 1.6 milliseconds. In addition the accuracy of measuring the position of a signal on the telemetering record was found to be $\pm$ 1 milliseconds.

The probable error in the lateral components of the coordinate data was found to be $\pm$ 0.001 inches; the error in the longitudinal component z, $\pm$ 0.026 inches.

8.2 The Error in θ_w

In the previous section it has been noted that large systematic errors in θ_w may possibly exist. The main contributions to this systematic error are: assumption of non-viscous medium (magnitude not known), assumption of right circular conical shock ($\pm$ 0.5°), correlation between signal and probe position and distortion of shock wave by probe (less than $\pm$ 0.5°).

The estimate of experimental probable errors varies somewhat with the method of calculating θ_w from the coordinate data.

8.21 Method 1

For small angles of yaw equations (14) and (15) of Section 7.3 were used. Thus, for either x or y equal to zero

$$\tan \theta_w = \frac{X}{z} \tag{21}$$

the relation for the propagation of independent errors is (R16).

$$P_f^2 = \left(\frac{\partial f}{\partial x}\right)^2 P_x^2 + \left(\frac{\partial f}{\partial y}\right)^2 P_y^2 + \cdots \tag{22}$$

where

$$f = f(x,y, \ldots)$$

thus we obtain

$$P_{\theta_w} = \frac{\cos^2 \theta_w}{z^2} \sqrt{z^2 P_x^2 + x^2 P_z^2} \text{ radians} \tag{23}$$

In a typical case (point 1 ↑) we have $\Theta_w = 27.72^o$, $x = 8.054"$, $z = 16.444"$; and since $P_x = \pm 0.001"$ and $P_z = \pm 0.026"$,

$$P_{\Theta_w} = \pm 0.035 \text{ degrees.}$$

If we average the angles obtained from the coordinates of four points on the conical surface then

$$P_{\Theta_{wav}} = \frac{P_{\Theta_w}}{2} = \pm 0.02 \text{ degrees.}$$

8.22 Method 2

The coordinates of three points on the cone's surface were used to calculate A, B, C from the three simultaneous equations obtained from equation (16)

$$x_1 A + y_1 B + z_1 C + \sqrt{x_1^2 + y_1^2 + z_1^2} = 0$$

$$x_2 A + y_2 B + z_2 C + \sqrt{x_2^2 + y_2^2 + z_2^2} = 0$$

$$x_3 A + y_3 B + z_3 C + \sqrt{x_3^2 \quad y_3^2 \quad z_3^2} = 0 \qquad \text{(16a)}$$

Θ_w is then found from the relation (17)

$$\cos \Theta_w = \frac{1}{\sqrt{A^2 + B^2 + C^2}} \qquad \text{(17a)}$$

The exact relation for P_{Θ_w} in this case is quite a long expression.

However in a typical case A and B are negligibly small compared to C; three of the six values of x and y are zero and the other three are approximately equal; and C is given by:

$$C = \frac{\cos \phi}{\cos \Theta_w}$$

where $\cos \phi$ is approximately unity. With these considerations

an approximate relation for P_{θ_w} is found to be:

$$P_{\theta_w} \cong \frac{\cos^2 \theta_w}{\sin \theta_w} P_c$$

where

$$P_c \cong \sqrt{2} \left[\frac{(z_4 + z_2)\left(\frac{z_4}{\alpha_4}\right) - (\alpha_4 + \alpha_2)}{(z_4 + z_2)^2} \right] P_z \qquad (24)$$

and

$$\alpha_i = \sqrt{x_i^2 + y_i^2 + z_i^2}$$

In a typical case (point 5↓) we have:

$$(x_1, y_1, z_1) = (7.963,\ 0,\ -15.63),\quad \theta_w = 26.70$$

$$(x_2, y_2, z_2) = (0,\ 7.960,\ -16.00)$$

$$(x_4, y_4, z_4) = (0,\ -7.957,\ -15.70),\quad P_z = \pm\ 0.026"$$

we find

$$P_{\theta_w} = \pm\ 0.027^o$$

§ .23 Method 3

The statistical adjustment of data gives a probable error based on external consistency, i.e., based on the "fit" of the adjusted conical surface with the observed data. The values obtained for the "two probe" data for which this type of calculation was made are shown in Table 9.

8.3 The Error in Temperature

Ambient air temperatures were calculated from the relation:

$$T = \left(\frac{V}{65.9M}\right)^2 \quad \text{Degrees Kelvin} \tag{20}$$

The M corresponding to a given value of Θ_W was taken from the tables of (R12) Applying equation (22) for the propagation of error we find:

$$P_T = 2T\sqrt{\left(\frac{P_V}{V}\right)^2 + \left(\frac{\partial M}{\partial \Theta_W}\frac{P_{\Theta_W}}{M}\right)^2} \tag{25}$$

Typical values of $\frac{\partial M}{\partial \Theta_W}$ are shown in Table 10. Values of P_T corresponding to the experimental errors in Θ_W are shown in Table 7.

The error in temperature due to one of the systematic errors that may exist is large. Neglecting error in velocity in equation (25), we find the error in temperature due to a systematic error in Θ_W to be:

$$P_T = \frac{2T}{M}\frac{\partial M}{\partial \Theta_W} P_{\Theta_W} \tag{25a}$$

For point (5†): $T = 255^\circ$, $M = 3.988$, $\frac{\partial M}{\partial \Theta_W} = 0.476$.

If $P_{\Theta_W} = 0.5^\circ$, then

$$P_T = 30^\circ$$

9. FUTURE PLANS

9.1 V-2 Number 56 Data Will Be Re-analyzed

The calculation of θ_w in this report is based on the assumption that the shock cone was a right circular cone. The angles will be recalculated using the elliptical cone of the second order theory.

9.2 The Assumption That Air is Non-viscous Will Be Investigated

In Section 3.12 it was noted that the assumption of zero boundary layer thickness is no longer valid when the air density decreases to a very low value at high altitudes.

Theoretical predictions of the effect of viscosity (reduced density) on conical flow theory is extremely difficult because the differential equations that describe the viscous flow are non-linear.

The most direct and accurate method of finding out the effect of reduced density on conical flow theory would be a model test in an ideal low density wind tunnel. Flight conditions at high altitudes would be simulated in such a wind tunnel. An experiment using existing facilities is being planned and will be carried out in the near future.

The effect can also be investigated on a rocket flight. A more elaborate system of probes will be used. Four probes which lie in the same plane, two on each side of the missile axis (see Fig. 36) will be used. It has been estimated from the theory (R22) that curvature of the shock wave is a consequence of low density. The probe configuration described above will be able to detect such curvature. If significant curvature is found, the present conical flow theory is not valid.

9.3 A Check Will Be Made on the Position of the Pirani Gauge Relative to the Shock Wave at the Time a Signal is Obtained

The model test described in Section 4 showed that the Pirani signal was obtained when some part of the tip of the probe first made contact with the shock wave. The accuracy of this experiment was estimated to be $\pm$ 0.5° (in terms of θ_w). This test will be repeated and an attempt made to improve the accuracy.

9.4 The Next Trial of the Method

The probe method will next be tried on an Aerobee rocket. Investigation of the stability of previous Aerobees was inconclusive.

As reported in (R5); "APL round A-10 had zenith angle not greater than 10° up to 234,000 feet, and less than 15° to 274,000 feet above msl." The effect of yaw would be considerable; second order theory would be used to calculate the resulting temperatures. It is planned to use more probes so that the elliptically shaped shock cone can be calculated accurately (see Fig. 36). The probe array will include those necessary for the measurement of curvature in the shock wave.

It is planned to fly a Doppler system similar to that used on V-2 Rockets, so that accurate velocity information will be available. The Pirani gauges and amplifier will be similar to those used on V-2 Number 56. Data will be recorded on magnetic tape with parachute recovery of the equipment.

There is considerable change in the mechanical design of the equipment because the Aerobee is a much smaller missile than the V-2.

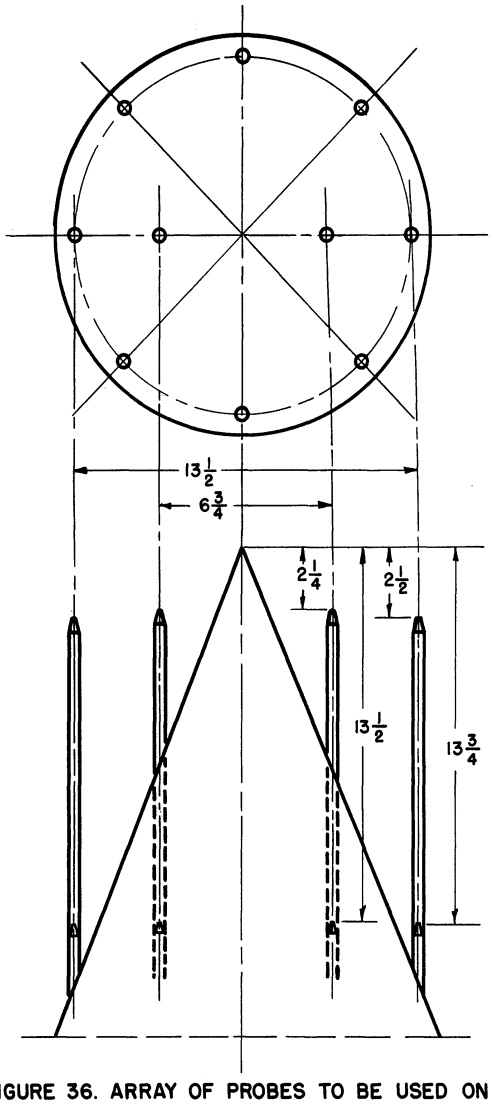

FIGURE 36. ARRAY OF PROBES TO BE USED ON NEXT TRIAL OF THE METHOD.

10. GENERAL DISCUSSION

10.1 Increased Precision at Lower Mach Numbers.

On V-2 Number 56 temperatures were measured for missile speeds in the range Mach 3.4 - 4.2. For a given error in θ_w, the error in temperature will be less for a lower speed missile such as the Aerobee. This can be checked with equation 25 and the values of $\frac{\partial M}{\partial \theta_w}\frac{1}{M}$ of Table 9. Velocity, obtained by Doppler, will have very small error, thus the error in temperature will be due mainly to the error in θ_w. Equation (25a) will apply, thus:

$$P_t = 2T \frac{\partial M}{\partial \theta_w}\frac{1}{M} P_{\theta_w} \qquad (25a)$$

and at a given temperature (for a given error in θ_w) the error in in temperature at Mach 3 is .65 times that at Mach 4; at Mach 2, only 0.29 times that at Mach 4.

10.2 The "Up-Down" Discrepancy

In Section 7.5 it was noted that the temperature points obtained when the probe moved up through the shock wave were consistently above those obtained when the probe moved back down through the shock wave (see Fig. 35). The reason for this is not known. It may be due to the assumption that the Pirani signal was obtained when some part of the probe tip first meets the shock wave. This assumption is to be checked by another wind tunnel test (see Section 9.3).

From Figure 35 and Table 7 we see that the discrepancy was smallest for the pair of points 3 ↓ and 4 ↑ , which are the points having the largest Mach number. At smaller Mach numbers and at higher altitudes the discrepancy is greater.

On the Aerobee, with smaller Mach numbers the discrepancy will not necessarily be larger, however, because of the increase in precision in temperature for a given error in θ_w (discussed in Section 10.1).

The discrepancy may be decreased by a change in the probe design (see next Section, 10.3)

10.3 Probe Development

It should be noted that there has been very little development work on probes for use in detecting the shock wave. Since the experiment is rocket borne it is difficult to reproduce in the laboratory the conditions which are met in flight. Development of the probes thus follows each flight. For example, the Pirani gauges used on V-2 Number 56 were made to be more rugged than those which failed on V-2 Number 50.

Several changes in the probes have been suggested by the

experience gained on V-2 Number 56. The tip of the gauge is to have a diameter only two-thirds that of the gauges used previously. This may reduce the "up-down" discrepancy discussed above. The Pirani gauge circuit will be modified so as to increase the sensitivity at low pressures at the expense of the sensitivity at high pressures. It is hoped that this will result in signals above 230,000 feet altitude (the altitude of the last signal obtained on V-2 Number 56).

10.4 Measurement of Winds in the Upper Atmosphere.

It is interesting to notice that with several assumptions the probe experiment can be used to measure winds in the upper atmosphere. The assumptions are:

(a) The wind is horizontal
(b) The attitude of the nose cone of the missile with respect to earth can be accurately determined.

In Figure 37 we have a right cartesian coordinate system (x,y,z) in space with the xy plane parallel to the plane which is tangent to the earth at the launching site. The vector A, with components (A_1, A_2, A_3) is the tangent to the trajectory of the missile at a given point in space, that is, the velocity vector of the missile with respect to earth. The vector B represents the axis of the nose cone, having direction cosines ($\beta_1, \beta_2, \beta_3$). If C is the free stream velocity vector of the missile, i.e., the velocity vector of the missile with respect to the air, then A-C is the wind velocity vector. The angle ϵ is the angle of yaw between the nose cone axis and the free stream velocity vector, while ϕ is the yaw angle between the nose cone axis and the axis of the shock wave. η is the angle between the x axis and the line in which the plane of yaw intersects the xy plane. In the following ($\gamma_1, \gamma_2, \gamma_3$) are the direction cosines of the vector C. (i, j, k) are unit vectors in the (x,y,z) directions respectively. The points A, B, C lie in a horizontal plane.

Analysis of the probe data will yield an angle of yaw ϕ (between nose cone axis and shock wave axis) as well as the shock wave angle θ_w. The orientation of the plane of yaw and thus η can be found if the attitude of the nose cone (direction cosines ($\beta_1, \beta_2, \beta_3$) and roll of the missile) is known. ϵ can be found from the relation

$$\epsilon = \frac{\phi}{1 - \alpha} \tag{18}$$

where α is a function of the Mach number. Mach number and thus α are found from (R13) when θ_w is known. Then:

$$\cos \epsilon = \beta_1 \gamma_1 + \beta_2 \gamma_2 + \beta_3 \gamma_3 \tag{26}$$

or

$$|C| \cdot \cos \epsilon = \beta_1 C_1 + \beta_2 C_2 + \beta_3 C_3 \tag{26a}$$

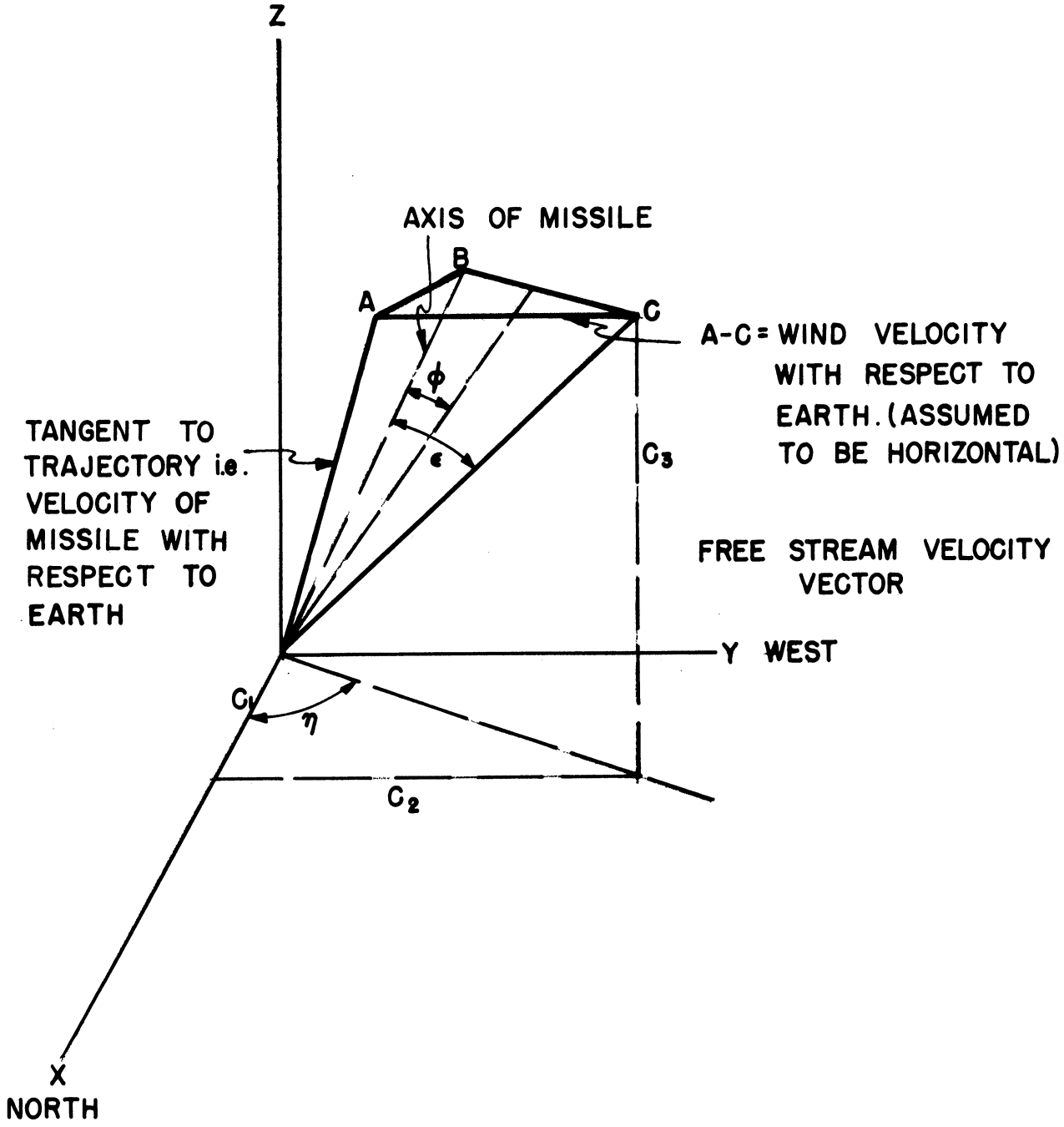

FIG. 37

ILLUSTRATION OF METHOD OF MEASURING UPPER ATMOSPHERE WINDS.

where

$$|C| = \sqrt{C_1^2 + C_2^2 + C_3^2} \tag{27}$$

also

$$\tan \eta = \frac{C_2}{C_1} \tag{28}$$

From these relations and the fact that $A_3 = C_3$ we can solve for C_1 and C_2. We find

$$C_1 = \left[\frac{\beta_3 \pm \sqrt{\frac{(\beta_3^2 - \cos^2\epsilon)\sec^2\eta}{(\beta_1 + \beta_2 \tan\eta)^2} + 1}}{\frac{\cos^2\epsilon \sec^2\eta}{(\beta_1 + \beta_2 \tan\eta)} - (\beta_1 + \beta_2 \tan\eta)} \right] A_3 \tag{29}$$

and

$$C_2 = C_1 \tan \eta \tag{30}$$

The wind vector is:

$$C - A = (C_1 - A_1)i + (C_2 - A_2)j \tag{31}$$

with magnitude

$$|W| = \sqrt{(C_1 - A_1)^2 + (C_2 - A_2)^2} \tag{31a}$$

It is estimated that ϵ can be measured accurately enough to insure that it will contribute only a small amount to the error in wind velocity. It will be necessary, however, to obtain very accurate missile attitude data if a reasonably accurate measurement of wind velocity is to be made.

11. REFERENCES

1. Delsasso, de Bey and Reuyl, "Full-Scale Free-Flight Ballistic Measurements of Guided Missiles," BRL, Aberdeen Proving Ground, Md.

2. Stone, A. H., "On Supersonic Flow Past a Slightly Yawing Cone," J. Math. Phys., 27, No. 1, 1948.
Taylor, G. I. and Maccoll, J. W., Proc. Roy. Soc. (A139) (1933) pp. 278-311. Maccoll, J. W., Proc. Roy. Soc. (A159) (1937) pp. 459-472.

3. Progress Report No. 10, "Atmospheric Phenomena at High Altitudes," October 15, 1948, Signal Corps Project No. 172B.

4. Progress Report No. 14, "Atmospheric Phenomena at High Altitudes," June 14, 1949, Signal Corps Project No. 172B.

5. Progress Report No. 17, "Atmospheric Phenomena at High Altitudes," February 13, 1950, Signal Corps Project No. 172B.

6. "An Evaluation of Shadowgraph and Schlieren Optical Methods for Determining Temperatures in the Upper Atmosphere," July 1, 1949, Signal Corps Project No. 172B.

7. Tsien, H. S., "Superaerodynamics, Mechanics of Rarefied Gases," J. Aero. Sci., 13, No. 12, 1946.

8. Roberts, H. E., "The Earth's Atmosphere," Aero. Eng. Rev., 8 No. 10, 1949.

9. Grimminger, G., "Analysis of Temperature, Pressure, and Density of the Atmosphere Extending to Extreme Altitudes," Table 13, Rand Corp., Santa Monica, Calif., November 1948.

10. R5, page 22

11. Newell, H. E. and Siry, J. W., Upper Atmosphere Report No. II, NRL Report No. R-3030, December 30, 1946.

12. "Tables of Supersonic Flow Around Cones," Center of Analysis Technical Report No. 1, M.I.T., Cambridge, Mass., (1947).

13. "Tables of Supersonic Flow Around Yawing Cones," Center of Analysis Technical Report No. 3, M.I.T., Cambridge, Mass., (1947).

14. "Tables of Supersonic Flow Around Cones of Large Yaw," Center of Analysis Technical Report No. 5, M.I.T., Cambridge, Mass., 1949.

15. Loeb, L. B., "Kinetic Theory of Gases," pp. 78-80, McGraw-Hill, 1927.

11. REFERENCES (Continued)

16. Deming, W. E., "Statistical Adjustment of Data," Wiley, Inc., 1943.

17. "Trajectory Data From Mitchell Theodolite Observations of A-4 (V-2) No. 56," BRL Technical Note No. 150, January 1950, Aberdeen Proving Ground, Md.

18. "Trajectory Data from Askania Camera Observations of A-4 (V-2) Round 56 Launched November 18, 1949," BRL Technical Note No. 162, Feb. 6, 1950, Aberdeen Proving Ground, Md.

19. Jeans, J., "An Introduction to the Kinetic Theory of Gases," The McMillan Company, 1940.

20. Warfield, G. N., "Tentative Tables for the Properties of the Upper Atmosphere," N.A.C.A. T.N. No. 1200, January 1947.

21. Whipple, F. L., "Meteors and the Earth's Upper Atmosphere," Rev. Mod. Phys. 15, No. 1, October 1943.

22. Fraser, L. W., and Ostrander, R. S., "A Photographic Method of Determining the Orientation of a Rocket," APL Section GM-603 Report, April 3, 1950.

23. Durand, W. F., Aerodynamic Theory, Vol. III, J. Springer, Berlin.

12. ACKNOWLEDGMENTS

The cooperation and support of the Meteorological Branch of the Signal Corps and of all agencies at White Sands Proving Ground is deeply appreciated. Thanks are due to the Applied Physics Laboratory of Johns Hopkins University for the use of films which they obtained with the modified K-25 camera flown on V-2 number 56, and to the Meteorological Branch of the Signal Corps for obtaining missile attitude data from these films. The use of the University of Michigan Engineering Research Institute wind tunnel made possible the model tests of the experiment.

Figure 17 is a Signal Corps Engineering Laboratories photograph.